Long-lived chondroprogenitors are generated by Gli1^{+} fetal-limb cells and are replenished upon cell-cycle arrest in the cartilage.

Xinli Qu[1¶], Ehsan Razmara[1¶], Chee Ho H'ng[1], Kailash K. Vinu[1], Luciano G. Martelotto[2,3], Magnus Zethoven[4], Fernando J. Rossello[5,6,7], Shanika L. Amarasinghe[1,8,9], David R. Powell[8,10], Alberto Rosello-Diez[1,11-13*]

[1]Australian Regenerative Medicine Institute, Monash University, Clayton, Victoria, Australia.

[2]University of Melbourne Centre For Cancer Research, The University of Melbourne, Melbourne, Victoria, Australia.

[3]Present address: Adelaide Centre for Epigenetics. South Australian immunoGENomics Cancer Institute. University of Adelaide, Adelaide, South Australia, Australia.

[4]Peter MacCallum Cancer Centre, Melbourne, Victoria, Australia.

[5]Murdoch Children's Research Institute, The Royal Children's Hospital, Melbourne, VIC 3052, Australia

[6]Novo Nordisk Foundation Center for Stem Cell Medicine, Murdoch Children's Research Institute, Melbourne, VIC 3052, Australia.

[7]Department of Clinical Pathology, University of Melbourne, Melbourne, VIC, Australia.

[8]Monash Genomics and Bioinformatics Platform, Monash University, Clayton, Victoria, Australia.

[9]Present address: Biomedicine Discovery Institute, Monash University, Clayton, Victoria, Australia.

[10]Monash eResearch Centre, Monash University, Clayton, Victoria, Australia.

[11]Department of Physiology, Development and Neuroscience, University of Cambridge, Cambridge, UK.

[12]Department of Genetics, University of Cambridge, Cambridge, UK.

[13]Centre for Trophoblast Research, University of Cambridge, Cambridge, UK.

[¶]Equal contribution

***Correspondence:**
ar2204@cam.ac.uk, alberto.rosellodiez@monash.edu

Keywords: Gli1, Pdgfra, growth plate, endochondral ossification, chondroprogenitors, long bones, limb growth, skeletal stem cells, perichondrium, catch-up growth, developmental robustness.

Abstract

The growth-plate cartilage of the developing long bones is a well-known system of spatially segregated stem/progenitor, transient amplifying and terminally differentiated cells. However, the regulation of the number and activity of long-lived cartilage progenitors (LLCPs) is poorly understood, despite its relevance for understanding human-height variation, the evolution of limb size and proportions and the aetiology of skeletal growth disorders. Moreover, whether their behaviour can adapt to developmental perturbations, generating robustness, has not been explored. Here, we show that Gli1$^+$ cells are the fetal precursors of postnatal LLCPs. Moreover, while during normal growth they remain mostly dormant until postnatal stages, in response to cartilage-targeted cell-cycle arrest they increase their cartilage contribution, compensating for the perturbation. We further show that, during the response to challenge, some of the reparative Gli1$^+$ cells originate from Pdgfra$^+$ cells outside the cartilage anlage. Elucidating how stromal cells become Gli1$^+$ LLCPs could shed light on developmental robustness and lead to growth-boosting therapies.

Introduction

Developmental systems often display remarkable robustness, that is, the ability to overcome challenges that affect cell function or viability[1]. Elucidating the mechanisms underlying robustness could improve our fundamental understanding of how individual cells integrate information and coordinate with their neighbours such that organ-level collective behaviours are achieved. Moreover, it could lead to growth-modulating therapies for congenital or acquired growth disorders. Long bones in the limbs are a powerful model to study growth regulation. They grow via a transient cartilage template that is progressively replaced by bone[2]. Cartilage cells (chondrocytes) undergo progressive end-to-centre differentiation, starting as resting/reserve chondrocytes that are progressively recruited into the proliferative pool (flat cells arrayed in columns), which eventually enlarge and differentiate to hypertrophic chondrocytes. Some hypertrophic chondrocytes die, while others transdifferentiate into osteoblasts (bone-laying cells) that replace the cartilage with bone, forming the primary ossification center[3,4]. Osteoblasts can also migrate, along with blood vessels, from the perichondrium[5], a connective tissue layer that surrounds the cartilage and has been shown to contain a stem-cell niche known as groove of Ranvier[6]. A secondary ossification centre (SOC) forms later (~postnatal day 7 in the mouse) at both ends of the skeletal element, so that the growth cartilage gets 'sandwiched' into a so-called growth plate by both ossification centres.

Maintaining the size and structure of the growth plate–in other words, the balance between cartilage generation and destruction–is critical to sustain bone growth over time and requires refined control mechanisms. The size of the proliferative zone is maintained approximately constant due to a well-described negative feedback loop between Indian hedgehog and Parathyroid hormone related peptide that balances proliferation and differentiation[3]. But other control mechanisms are less known, especially regarding the resting-to-proliferative transition. In fetuses and neonates, cartilage progenitors (CPs) located in the reserve zone do not self renew[7], so that when one is recruited into a proliferative column, its lineage gets rapidly exhausted, leading to short clonal columns. At approximately three weeks of age, CPs start to self-renew–possibly in response to SOC signals–giving rise to long clonal columns (Ext. Data Fig. 1)[7]. These long-lived CPs (LLCPs) are the key driver of subsequent growth and therefore of final bone length. Therefore, elucidating their origin and regulation is critical to understanding normal and compensatory growth, as well as skeletal growth disorders and the evolution of limb size. One of the biggest unresolved questions is whether postnatal LLCPs arise from fetal short-lived ones, in response to intrinsic and/or extrinsic triggers (Ext. Data Fig. 1a), or whether they are already present but inactive in the fetal limb, becoming activated (or even recruited from outside the cartilage) in response to cartilage maturation (Ext. Data Fig. 1b). Determining which of these mechanisms take place during

normal growth, and whether they can adapt in response to developmental perturbations, is desirable for the development of targeted growth therapies, focussed on stimulating the expansion of the pool of LLCPs at the right time and location. In this study, we probed the system using models of cartilage-targeted cell-cycle arrest, combined with lineage tracing and functional analyses. We found that Gli1^{+} cells in the fetal limb give rise to dormant CPs, which later postnatally give rise to most of the chondrocytes of the growth plate. Moreover, these progenitors can be precociously activated by cartilage-targeted growth challenges, revealing significant plasticity and a strong reparative potential. We posit that this fundamental knowledge will be critical to understanding and manipulating cartilage growth and repair.

84 **Results**

85 *Mosaic cell-cycle arrest in the fetal cartilage triggers a compensatory response from Gli1^{+} cells.*

86 We previously generated a fetal mouse model of left-cartilage targeted, mosaic overexpression of p21
87 (which blocks the cell cycle in G1 phase[8]), by combining *Pitx2-Cre*[9], *Col2a1-rtTA*[10] and *Tigre*$^{Dragon\text{-}p21}$
88 alleles[11] (Ext. Data Fig. 2a, *Left-Cart-p21*^{MOE} model hereafter). In that study, we showed that the mosaic
89 cell-cycle arrest was compensated by hyperproliferation of the spared (p21^{-}) chondrocytes[11]. We
90 reasoned that, if short-lived CPs were the only source of LLCPs (as in Ext. Data Fig. 1a), their hastened
91 proliferation would lead to premature exhaustion of the CP pool (Ext. Data Fig. 2b), and therefore to
92 reduced bone length in the long term. To test this hypothesis, we followed mice from the *Left-Cart-*
93 *p21*^{MOE} model until postnatal day (P) 100, well beyond the end of the growth period. Interestingly, no
94 major asymmetries in bone length were found as compared to *Pitx2-Cre/+; Tigre*$^{Dragon\text{-}p21/+}$ mice
95 (Controls, Ctl hereafter, Ext. Data Fig. 2c, the left/right ratio was not significantly different for the tibia,
96 and only ~1.5% lower for the femur). This result suggested that either the spared resident CPs in the
97 *Left-Cart-p21*^{MOE} acquired self-renewing properties precociously, or that facultative CPs (i.e. cells that
98 would not normally contribute to cartilage at that age) were recruited to the challenged cartilage. To shed
99 light into this process, we undertook an unbiased single-nuclei RNA-seq approach of left and right fetal
100 knees from two E16.5 Ctl and two *Left-Cart-p21*^{MOE} embryos (Fig. 1a and Ext. Data Fig. 3a). Out of the
101 original dataset (~32,000 nuclei in 32 clusters, Ext. Data Fig. 3b, d), which contained mostly lateral plate
102 mesoderm-derived cells, and a minority of muscle and endothelial cells, we further explored the former
103 population (~21,000 nuclei, Ext. Data Fig. 3d'). This subset was composed of 23 clusters (Ext. Data Fig.
104 3c, d), which we grouped in five main categories (see Methods): chondrocytes (Ext. Data Fig. 3b'),
105 tenocytes, fibroblasts, perichondrium and joint-associated mesenchymal cells. Analysis of regulon
106 activity with SCENIC[12] revealed that the activity of GLI-Kruppel family member 1 (GLI1) transcription
107 factor was significantly upregulated in the left experimental (ExpL) osteochondroprogenitors and to a
108 lesser extent in resting chondrocytes (Fig. 1a'). This was interesting because Gli1^{+} osteochondro-
109 progenitors have been shown to participate in the repair of bone fractures[13]. Thus, we next asked whether
110 the number of Gli1^{+} cells changed in response to cartilage-targeted p21 overexpression. Indeed, the
111 Propeller tool[14] revealed that, within the Gli1^{high} lateral-plate-mesoderm-derived population, the
112 proportion of cells belonging to the chondrocyte group was increased in experimental limbs, as
113 compared to Ctl (Ext. Data Fig. 3e,e'). To confirm these findings, we turned to Cre-based lineage tracing.
114 To trace the Gli1-lineage independently of p21 expression, we utilised a Doxycycline (Dox)-controlled,
115 Cre-independent p21 expression system, targeted to all cartilage elements (*Col2a1-rtTA/+; Tigre*$^{TRE\text{-}p21/+}$,
116 *Pan-Cart-p21*^{MOE} model hereafter; TRE, Tet-responsive element)[15]. Females bearing a tamoxifen

117 (TM)-inducible Cre recombinase (CreER^{T2}) cassette[16] targeted to the *Gli1* locus (*Gli1^{CreER}* hereafter)
118 were crossed with *Pan-Cart-p21^{MOE}* males bearing also a Cre-reporter cassette (lox-STOP-lox-
119 tdTomato) targeted to the safe harbour locus *Rosa26* (*R26$^{LSL\text{-}tdTom}$* hereafter, Fig. 1b)[17] and given Dox at
120 embryonic day (E) 12.5 and TM at E13.5. As with the model targeted to the left limb, we confirmed that
121 expression of p21 in 60-70% of chondrocytes (Ext. Data Fig. 4a) did not cause growth defects by
122 postnatal day (P) 0 (Fig. 1b'). Despite continuous Dox exposure, the fraction of p21^{+} chondrocytes
123 decreased with time (Ext. Data Fig. 4a), as we previously described with the *Left-Cart-p21^{MOE}* model[11].
124 To assess the involvement of Gli1^{+} cells in this compensatory response, we followed the distribution of
125 tdTom^{+} cells inside and outside the cartilage 1, 4, 7 days post TM (dpt, Fig. 1c,c'). In *Pan-Cart-p21^{MOE}*
126 mice, the Gli1-lineage showed a significant cartilage expansion, as compared to controls, at all stages
127 analysed (Fig. 1c'). These results suggested that, in control conditions, most E13.5-marked Gli1-derived
128 chondrocytes only contribute transiently and are then "pushed out" of the cartilage, while in *Pan-Cart-*
129 *p21^{MOE}* limbs, the Gli1-lineage increases its contribution to longer-lived CPs. Given that CPs reside in
130 the resting zone[18], we divided the cartilage analysis into resting and proliferative, finding that both zones
131 showed increased number of tdTom^{+} cells, typically biased towards the resting zone (Ext. Data Fig. 4b-
132 b''). Moreover, the contribution outside the cartilage was also expanded in P0 *Pan-Cart-p21^{MOE}* limbs
133 compared to controls (Fig. 1c'), suggesting that the challenged cartilage signals to the surrounding
134 tissues.
135 Importantly, since our initial labelling of the Gli1-lineage (E13.5-TM) was done after the induction of
136 p21 expression (E12.5), we were not able to distinguish between two scenarios: i) all the Gli1^{+} cells
137 derive from formerly Gli1^{+} cells; ii) *Gli1* expression is activated *de novo* in cells that were Gli1^{-} before.
138 Since the second scenario would reveal an unknown degree of plasticity that could be relevant for the
139 understanding of growth control and the design of future therapies, we decided to further investigate this
140 matter. We reasoned that, by providing Dox and TM both at E12.5, most of the tdTom-labelling would
141 happen among existing Gli1^{+} cells, with most of the TM being washed out by the time any potential *de*
142 *novo* expression of Gli1 took place. Using this approach, we found that the number of descendants was
143 lower in P0 *Pan-Cart-p21^{MOE}* as compared to E12.5-Dox/E13.5-TM (Ext. Data Fig. 4c-c'). This result
144 suggests that while the existing population of Gli1^{+} cells contributes to the repair, some Gli1^{-} cells
145 become Gli1^{+} <u>after</u> *p21* induction in the cartilage.
146

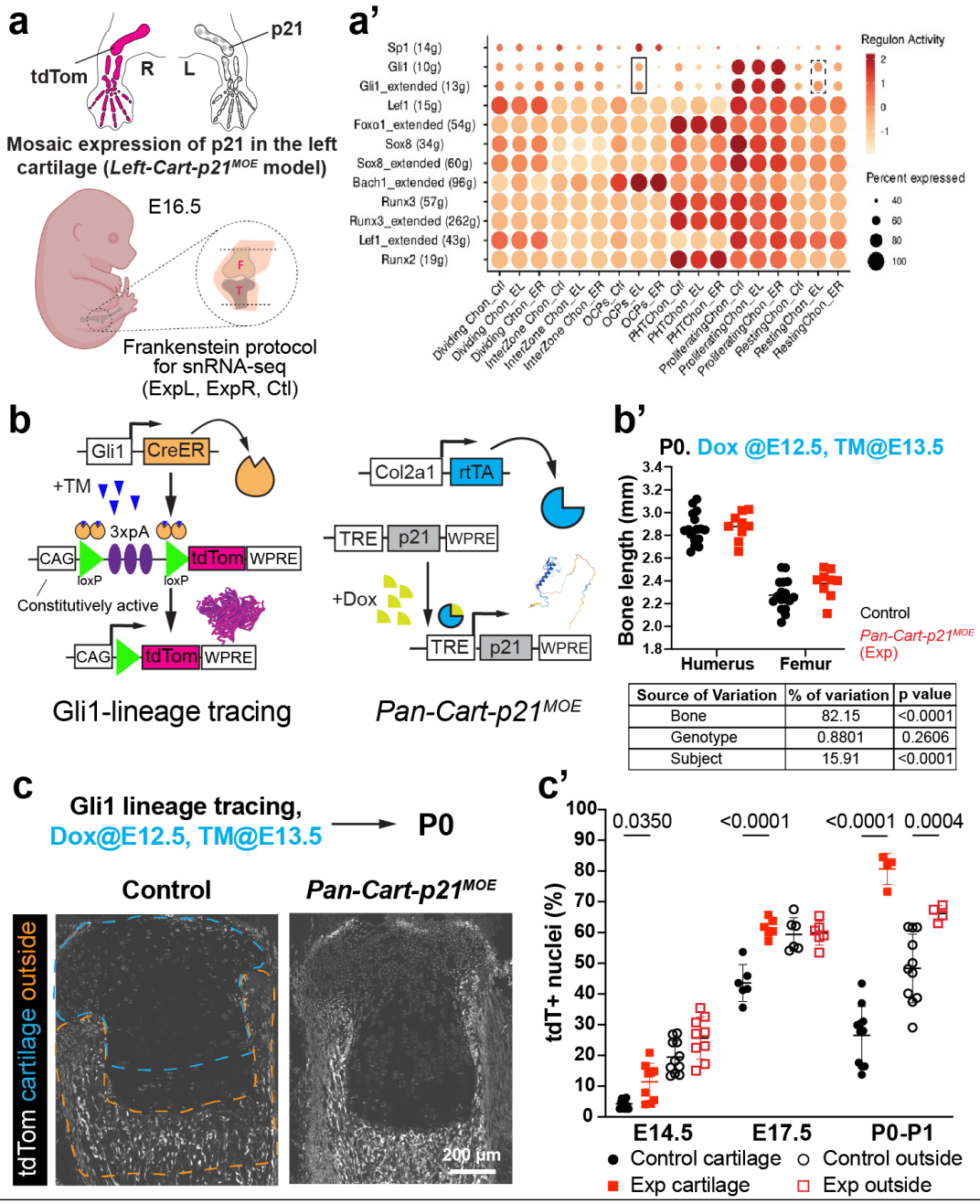

Source of Variation	% of variation	p value
Bone	82.15	<0.0001
Genotype	0.8801	0.2606
Subject	15.91	<0.0001

Figure 1. Mosaic cell-cycle arrest in the fetal cartilage triggers compensation from Gli1^{+} stromal cells. a, a', A left-specific, cartilage-targeted p21 mosaic over-expression model (*Left-Cart-p21^{MOE}*) was used for snRNA-seq analysis of knees. Left (L) and right (R) knees were processed separately but analysed together in control embryos (a). Chondrocyte-related cells were analysed via SCENIC and relevant regulons are shown boxed (a', dashed lines denote mild changes). **b, b'**, Expression of p21 in the cartilage, induced from E12.5 to P0 (b), does not lead to growth defects (b'). The table shows results of 2-way ANOVA. **c, c'**, The Gli1 lineage was followed in absence (Control) and presence of p21 misexpression (*Pan-Cart-p21^{MOE}*), and quantified in the regions shown in (c). In c', data shown as mean± SD. p-values for Sidak's multiple comparisons test after 2-way ANOVA are shown.

To test whether Gli1-derived chondrocytes are required for the compensation of *Pan-Cart-p21^{MOE}*, we used a *Tigre$^{Dragon\text{-}aDTA}$* allele in which inducible expression of aDTA (attenuated diphtheria toxin) requires Cre and rtTA activity[15,19] (Fig. 2a). Mice were crossed as shown in Fig. 2a to generate

156 *Gli1*$^{CreER/+}$; *Col2a1-rtTA/+; Tigre*$^{TRE\text{-}p21/+}$ embryos (phenotypically akin to *Pan-Cart-p21*^{MOE}) and
157 *Gli1*$^{CreER/+}$; *Col2a1-rtTA/+; Tigre*$^{Dragon\text{-}aDTA/TRE\text{-}p21}$ littermates (*Pan-Cart-p21*^{MOE}*; Gli-Cart-DTA,* Fig.
158 2a), in addition to control (rtTA^{-}) ones. We gave Dox from E12.5 till sample collection to induce p21
159 expression in the cartilage (*Pan-Cart-p21*^{MOE}), and TM at E13.5 to induce cell death of the rtTA-
160 expressing Gli1-derived chondrocytes (*Gli-Cart-DTA* combination). As predicted, TUNEL staining
161 revealed apoptosis only in the cartilage of *Pan-Cart-p21*^{MOE}*; Gli-Cart-DTA* embryos (Fig. 2b, b'). We
162 then measured bone length at P0 and found that bone growth was impaired in *Pan-Cart-p21*^{MOE}*; Gli-*
163 *Cart-DTA* pups as compared to *Pan-Cart-p21*^{MOE} and/or control pups (Fig. 2c). This result demonstrates
164 that Gli1-derived chondrocytes are required in the E13.5 to P0 period to compensate for cell-cycle arrest
165 in the cartilage. Of note, due to increased mortality of *Pan-Cart-p21*^{MOE}*; Gli1-Cart-DTA* mice, later time
166 points could not be analysed.

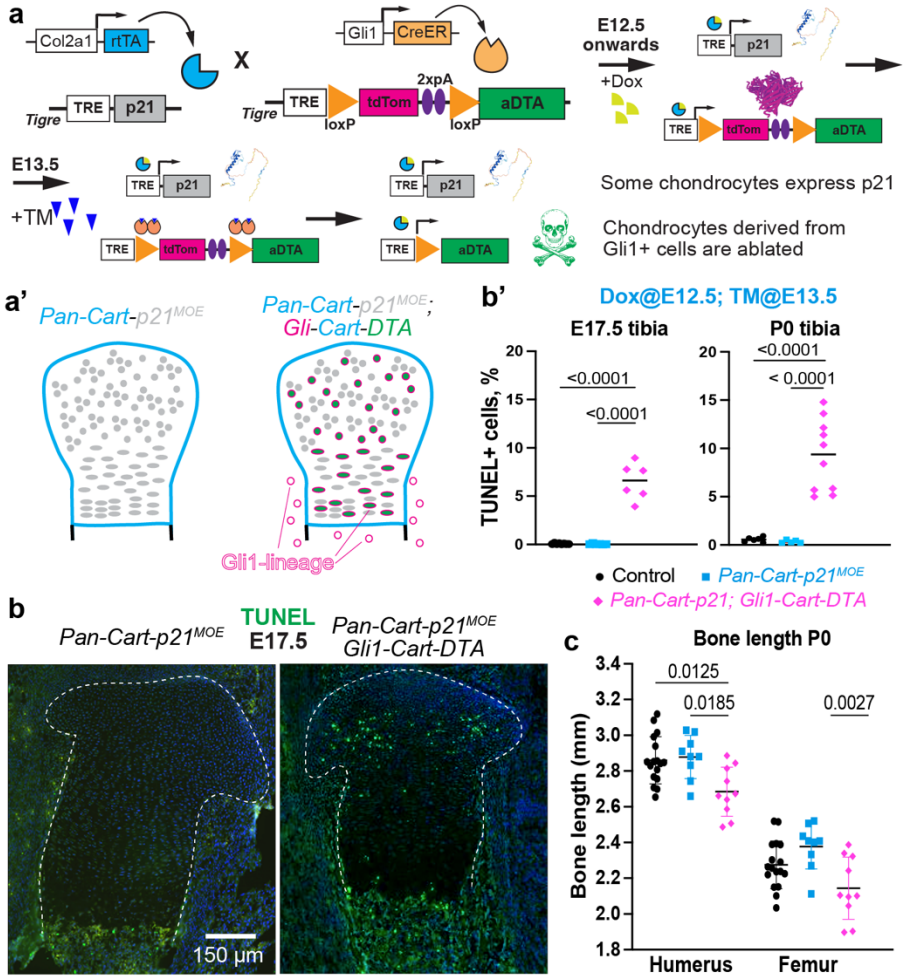

167
168 **Figure 2. Gli1-derived chondrocytes are needed for compensation of *Pan-Cart-p21*^{MOE}. a**, A *Dragon-aDTA* allele (aDTA= attenuated diphtheria toxin) is combined with *Gli1*^{CreER} and *Pan-Cart-p21*^{MOE} to ablate Gli1-derived chondrocytes during p21-induced compensation. **b, b'**, Example images of TUNEL (b, cartilage outlined) and quantification (b') for the indicated stages and genotypes (n=8,6,6 at E17.5, n=6,5,10 at P0). Significant p-values for Tukey's test after ANOVA are shown. **c**, Length of the P0 mineralised region is shown for the indicated genotypes as mean ±SD (n=17, 9, 10). Significant p-values of Sidak's multiple comparisons test (after 2-way ANOVA) are shown.

169 *Fetal Gli1$^+$ cells give rise to most chondrocytes in the juvenile and adult growth plate*

170 Having identified a highly-reparative fetal Gli1$^+$ population, we set out to determine their role during
171 normal growth. When Gli1$^+$ cells are lineage-traced at one month of age, they label 60-80% of
172 chondrocytes of the growth plate one month later[20], indicating that P30 Gli1$^+$ chondrocytes contain long-
173 lived chondroprogenitors (LLCPs). Since Gli1$^+$ cells exist in the limb at fetal stages (Ext. Data Fig. 5a,
174 a'), we tested whether fetal Gli1$^+$ cells already contained LLCPs. We crossed *Gli1$^{CreER/CreER}$* females
175 with *R26$^{LSL\text{-}tdTom/LSL\text{-}tdTom}$* males and provided TM at either E12.5 or E13.5 and quantified the number of
176 tdTom$^+$ cells at multiple stages (E14.5, E17.5, E19.5 and P30 and P60). In all cases, tdTom$^+$ cells were
177 found both inside the cartilage and adjacent tissues, including perichondrium, metaphysis, interzone
178 knee region and SOC (Fig. 3a, a'). Since fetal CPs had been shown not to self-renew[7], we expected the
179 % of labelled chondrocytes to decrease with time. On the contrary, the contribution of Gli1-lineage cells
180 to the cartilage increased with time, labelling up to 65-70% of chondrocytes in the 2-month-old growth
181 plate (Fig. 3b). To ascertain when in this process Gli1-derived chondrocytes switched from forming
182 short to forming long clonal columns, we used a tri-colour reporter line (RGBow, Fig. 3c)[21] that
183 randomly expresses one of three membrane-bound fluorescent proteins upon Cre-recombination. After
184 giving TM at E12.5 or E13.5, we analysed the number, location and length of distinct columns in the
185 three regions of the cartilage. Notably, the total number of columns increased up to P0-P1, the majority
186 located in the resting and proliferative zones (Fig. 3c, c'') and composed of 2-3 cells (Fig. 3d). By P14,
187 the total number of columns was significantly reduced but started to become longer (Fig. 3c'', d). By
188 P30 few columns remained, but many crossed the whole growth plate starting from the RZ (Fig. 3c',
189 c''). In summary, the results indicated that Gli1$^+$ cells at E12.5 or E13.5 give rise to CPs with two
190 different fates: short-lived clones that get depleted over time, and long-lived ones that remain dormant
191 at peri-natal stages and become more active after the second postnatal week.

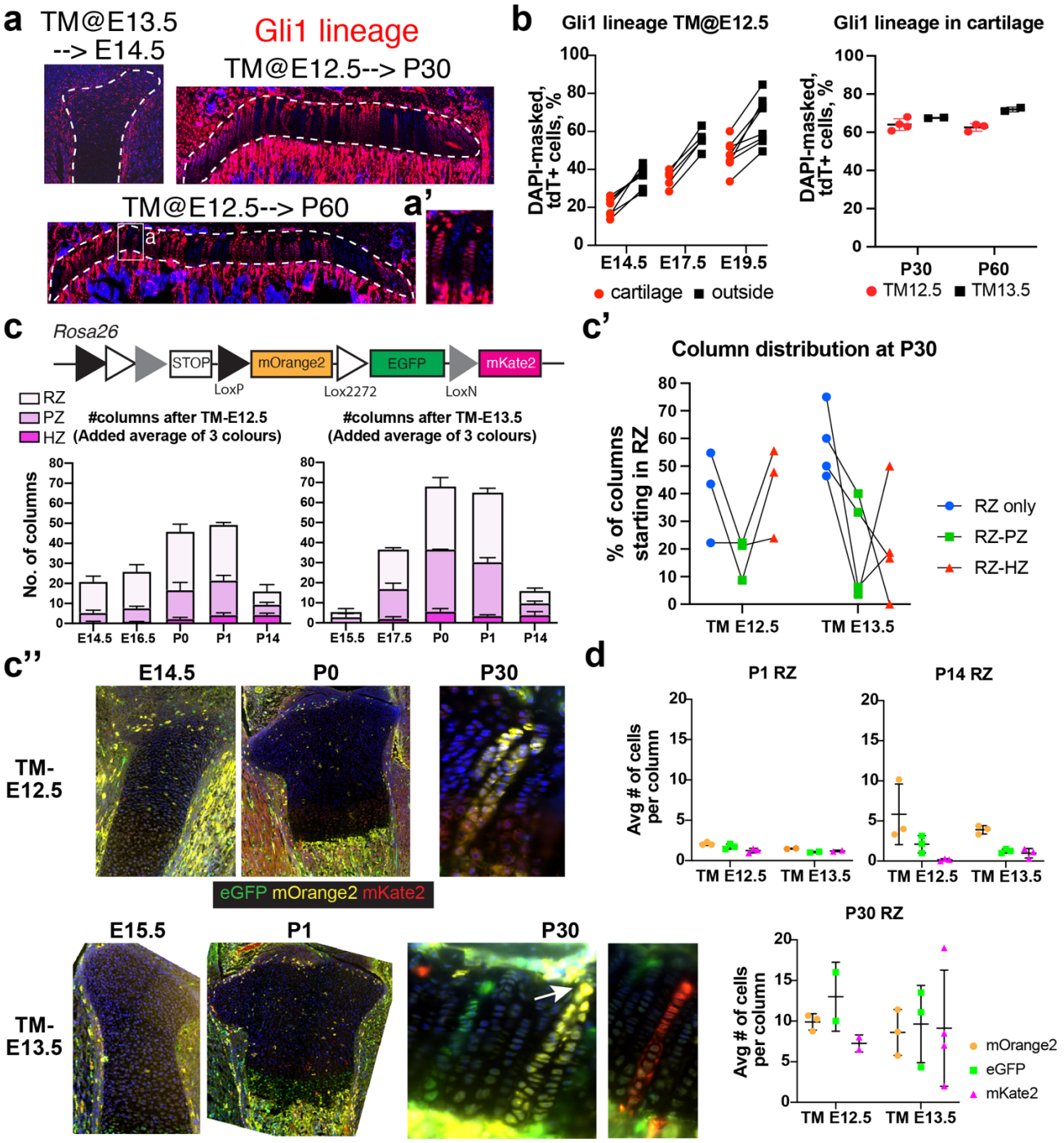

Figure 3. Fetal Gli1$^+$ cells give rise to most chondrocytes in the juvenile and adult growth plate. a, Examples of Gli1-lineage tracing after TM induction at E12.5 or E13.5, analysed at the indicated stages. **b**, Quantification of reporter-expressing cells, inside and outside the cartilage for TM-E12.5 (left, n=6, 5, 6), or in cartilage for both inductions (right, n=4, 2). **c-c''**, The tri-colour reporter RGBow was used to quantify individual clones in the growth plate (c, added average of each colour is shown), at multiple times post induction (n=3, 4, 3, 3, 3, 3 for TM-E12.5, n=3, 3, 2, 2, 2, 3, 3 for TM-E13.5). RZ, PZ, HZ: resting, proliferative, hypertrophic zone. In c', the % of P30 columns starting from RZ are shown, based on where they end (n= 3 and 4). c'' shows representative images. Arrow: RZ-rooted LLCP. **d**, number of cells per RZ-rooted column, for the stages and induction times indicated.

198 *Long-lived CPs are derived from Gli1^{+} cells that continuously seed the fetal and perinatal cartilage*

199 We next asked whether Gli1-derived LLCPs were already present in the early cartilage template (around
200 E12.5), or whether they were incorporated later from the adjacent tissues. The latter possibility is
201 supported by studies showing that the chicken perichondrium is a reservoir for cartilage precursors[22]. To
202 this end, we generated a mouse line in which expression of nuclear-directed Green Lantern fluorescent
203 protein depends on Dox-activated rtTA (Fig. 4a and Ext. Data Fig. 6a-b, *Tigre$^{TRE\text{-}nGL}$* hereafter). We then
204 crossed *Gli1$^{CreER/CreER}$; Tigre$^{TRE\text{-}nGL/TRE\text{-}nGL}$* females with *Col2a1-rtTA/+; R26$^{LSL\text{-}tdTom/LSL\text{-}tdTom}$* males, and
205 provided TM at E13.5 to label the Gli1 lineage with tdTom, and a 1-day pulse of Dox to transiently
206 express nGL primarily in fetal chondrocytes. We then followed the green signal over time, with the
207 expectation that quiescent chondrocytes (that is, the cells that will become LLCPs) would retain
208 fluorescence for longer than cells dividing quickly (Fig. 4a). Moreover, by providing Dox at different
209 points, we aimed to label different potential CP populations (Fig. 4a'): those already resident in the early
210 cartilage anlage (Dox at E12.5), and those seeded later into the cartilage (Dox at E17.5). Most green
211 cells after E12.5-Dox were found inside the cartilage, with a negligible number in the perichondrium
212 (Fig. 4a'', Ext. Data Fig. 6c-c'), confirming that the new tool could be used to track cells located only
213 in the cartilage. As predicted, the number of GL^{+} chondrocytes dropped fast at first (~2.5-fold from
214 E17.5 to E19.5), but then stabilised at 2-3% of the RZ cells at P14 and P21 (Fig. 4b, no green signal in
215 the PZ), becoming undetectable by P30. Remarkably, the % of Gli1-lineage chondrocytes in the GL^{+}
216 population increased over time in the RZ (Fig. 4d), until ~90% of GL-retaining CPs at P14 belonged to
217 the E13.5-labelled Gli1-lineage. Conversely, only ~3% of the Gli1-lineage cells in the P14 RZ were also
218 GL^{+}, indicating that the Gli1-lineage contains other subpopulations (Fig. 4e). Similar results were
219 obtained when Dox was given between E17.5 and E18.5 (e.g. Fig. 4b', c, d', e'), except for the proportion
220 of GL^{+} cells within the Gli1-lineage RZ chondrocytes (~6.7% at P21). These results suggested that while
221 many LLCPs are already present in the E12.5 cartilage, more LLCPs are added later, in both cases
222 derived mostly from fetal Gli1^{+} cells. To test this prediction, we extended the Dox pulse from E12.5 to
223 E18.5, so that newly added chondrocyte waves were also labelled. As predicted, many more double
224 positive cells were found in the P14 RZ than with any other regimen (Fig. 4b'', c, d'', e''), suggesting
225 that from E12.5 to E18.5 there is a continuous addition of LLCP precursors from outside the cartilage.

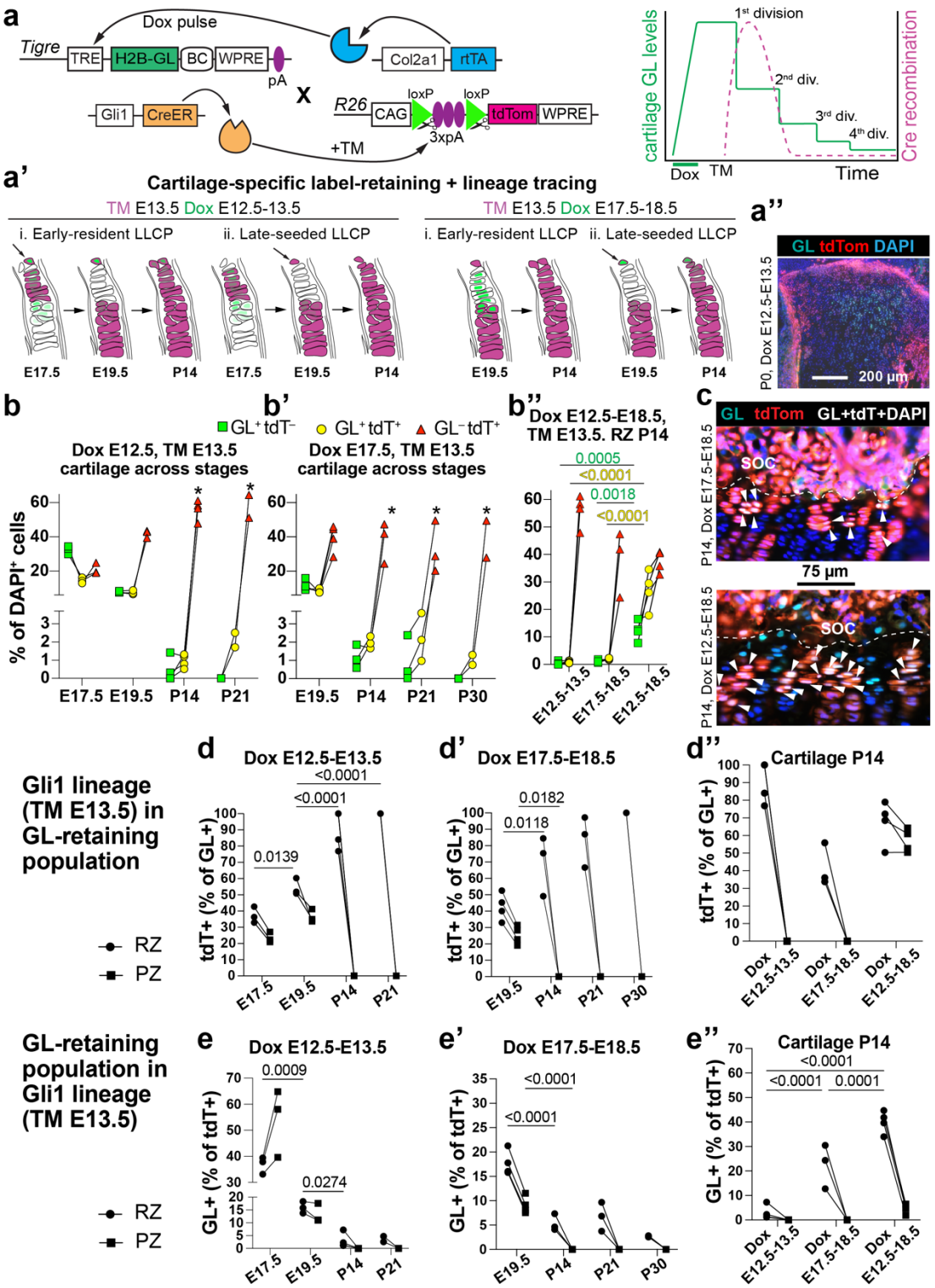

Figure 4. Most fetal LLCPs belong to the Gli1 lineage. **a-a''**, Model to permanently label the Gli1 lineage and transiently label chondrocytes with a nuclear GreenLantern (H2B-GL) that gets halved every cell division (a); different outcomes depending on Dox timing (a') and a representative image of the distribution after early labelling (a''). BC, barcoding region (not used here). **b-b''**, Quantification of single-positive and double-positive populations in the cartilage at the indicated stages after induction at E12.5-E13.5 (b, n=3, 3, 4, 2), E17.5-E18.5 (b', n=4, 3, 3, 2) or E12.5-E18.5 (b'', n=4). *: quantified in resting zone only. **c**, Representative images of tdT and nGL overlap (arrowheads) at P14 with 2 different induction regimes. SOC, secondary ossification centre (separated from cartilage by dashed lines). **d-e''**, % of tdT^+ cells within the GL^+ population (d-d'') or GL^+ cells within the tdT^+ population (e-e'') after 1-day Dox pulse at E12.5 (d, e) or E17.5 (d', e') or 6-day pulse at E12.5 (d'', e''). In all graphs p-values for multiple comparisons tests after 2-way ANOVA are shown.

Chondrocytes generated in the last postnatal week from Gli1+ cells are required for long-term bone growth

To test if Gli1-derived chondrocytes are required to sustain bone growth, we crossed *Gli1*^{CreER}; *Tigre* $^{Dragon\text{-}aDTA}$ mice with *Col2a1-rtTA; R26*$^{LSL\text{-}tdTom}$, and gave TM at E13.5 and Dox E12.5-P0. This way, only chondrocytes were ablated among Gli1-descendants (Fig. 5a-b'). While the ablation was incomplete and only sustained for a short time, this targeted injury led to reduced bone length by P100, especially for the tibia (Fig. 5c). This revealed the important role of fetal/perinatal Gli1-derived chondrocytes in long-term bone growth. Of note, ablation could not be sustained postnatally due to insufficient activity of *Col2a1-rtTA*, raising the possibility that partial compensation had taken place postnatally.

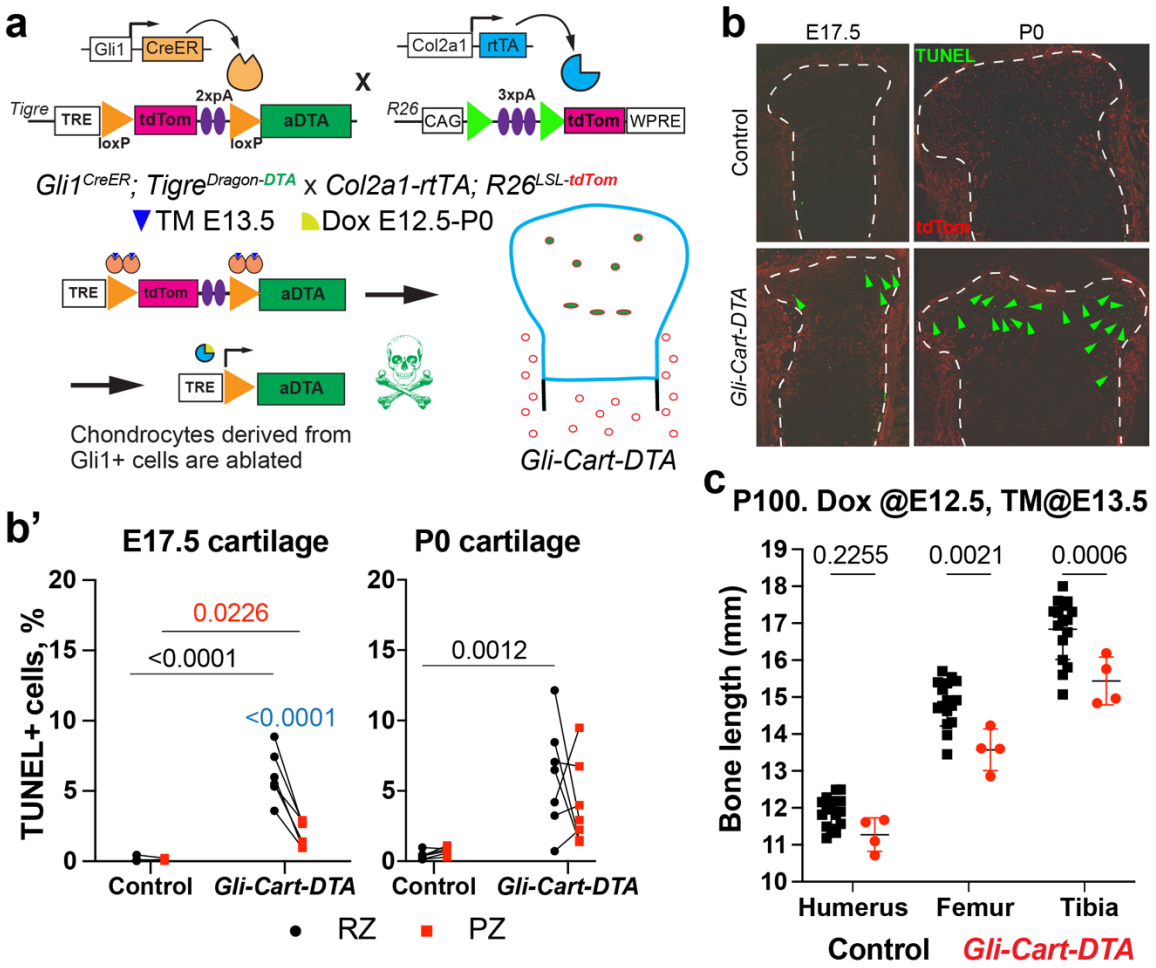

Figure 5. a The *Dragon-aDTA* allele was combined with *Gli1*^{CreER} and *Col2a1-rtTA* to activate diphtheria toxin expression exclusively in Gli1-lineage chondrocytes in the last week of gestation (*Gli-Cart-DTA* model). **b**, **b'** Typical images (b) and quantification (b') of TUNEL^{+} cells (arrowheads) at the indicated stages. **c** Bone length of Ctl and *Gli-Cart-DTA* mice at postnatal day 100 (P100). In b' and c, p-values of multiple comparisons tests after 2-way ANOVA are shown. RZ, PZ: resting proliferative zone.

243 *Some of the Gli1⁺ LLCPs generated upon challenge derive from stromal Pdgfra⁺ cells*

244 Having found evidence suggesting that stromal (non-cartilage) Gli1⁺ cells can become LLCPs (Fig. 4),
245 and that some Gli1⁻ cells become Gli1⁺ upon p21 misexpression (Ext. Data Fig. 4), we next set out to
246 determine the origin and regulation of Gli1⁺ cells in normal and challenged growth.

247 To capture the potential arising of new Gli1⁺ chondrocytes from stromal cells, we chose *platelet derived*
248 *growth factor alpha* (*Pdgfra*) as a marker of stromal cells that is not expressed in the cartilage (Ext. Data
249 Fig. 5b, b'). We crossed *Pdgfra*$^{CreER/+}$ females[23] with *Pan-Cart-p21*^{MOE}; *R26*$^{LSL\text{-}tdT/LSL\text{-}tdT}$ males and
250 provided Dox at E12.5 and TM at E13.5. We found that, in normal growth, the E13.5-labelled Pdgfra-
251 lineage gave rise to an increasing proportion of chondrocytes (Fig. 6a, 30-40% at E14.5, 45-50% at
252 E17.5 and ~60% at P0), strongly suggesting that the surrounding tissues can contribute to cartilage.
253 Moreover, the proportion of Pdgfra-lineage chondrocytes was progressively increased in *Pan-Cart-*
254 *p21*^{MOE} limbs as compared to controls (Fig. 6a, compare P0 with E14.5). Of note, the Pdgfra-lineage
255 located in the resting zone showed increased proliferation in *Pan-Cart-p21*^{MOE} vs. control limbs at E14.5
256 and E17.5 (Ext. Data Fig. 7a-b'), potentially explaining the progressive expansion observed at and after
257 E17.5 (Fig. 6a).

258 To determine to what extent Pdgfra-lineage expansion was related to the expression of *Gli1* in cartilage
259 cells, we analysed the overlap of tdTom (marking the Pdgfra-lineage) and *Gli1* expression in these cells
260 at E17.5 (Fig. 6b). While the proportion of *Gli1*⁺ cells within the Pdgfra-lineage was increased from
261 ~40% in controls to nearly 60% in *Pan-Cart-p21*^{MOE} samples (Fig. 6b' squares), the proportion of
262 Pdgfra-lineage cells within the Gli1⁺ population was slightly decreased from ~70% to 55% (Fig. 6b'
263 circles). This suggests that the expansion of Gli1⁺ cells in the cartilage was due to cells residing both
264 inside and outside the cartilage at the time of the insult. In summary, the number of Gli1⁺ chondrocytes–
265 belonging to both the Pdgfra-lineage and the non-Pdgfra-lineage–was increased, unlike the Gli1⁻ Pdgfra-
266 lineage, which remained the same in *Pan-Cart-p21*^{MOE} as compared to controls (Fig. 6c).

267 Although *Pdgfra* mRNA levels were somewhat decreased in *Left-Cart-p21*^{MOE} cartilage as compared to
268 controls (Ext. Data Fig. 5c), we reasoned that chondrocytes that had recently formed from Pdgfra⁺ cells
269 in response to cell-cycle arrest would retain PDGFRA protein for some time. Therefore, to further
270 explore Gli1⁺ chondrocytes as derivatives of the Pdgfra-lineage, we analysed PDGFRA protein
271 expression within and outside the Gli1-lineage at E14.5, i.e., shortly after p21 induction (Fig. 6d).
272 Indeed, the number of PDGFRA⁺ cells was increased within the Gli1-lineage cartilage in *Pan-Cart-*
273 *p21*^{MOE} as compared to controls (Fig. 6d' circles). In fact, the population that expanded the most in the
274 *Pan-Cart-p21*^{MOE} vs. control cartilage was the PDGFRA⁺ Gli1-lineage one (Fig. 6e), suggesting that this

275 population is especially involved in the repair. In summary, our data suggests that Pdgfra^{+} cells (mostly
276 located outside the cartilage) become Gli1^{+} CPs and progressively increase their contribution to cartilage
277 in *Pan-Cart-p21^{MOE}* limbs as compared to controls, contributing to the compensation. Lastly, we
278 examined the behaviour of the Pdgfra-lineage in long-term normal growth. Tracing of fetal Pdgfra^{+} cells
279 with the RGBow reporter during normal growth led to very few long columns being labelled at P30 (Fig.
280 6f, compare with 3c'), with most of the few long columns being restricted to the periphery of the growth
281 plate (Ext. Data Fig. 7c-d'). This suggests that Pdgfra^{+} cells do not give raise to a significant number of
282 Gli1^{+} LLCPs unless the cartilage is challenged. This begged the question of what the molecular changes
283 triggered by the challenge were.
284

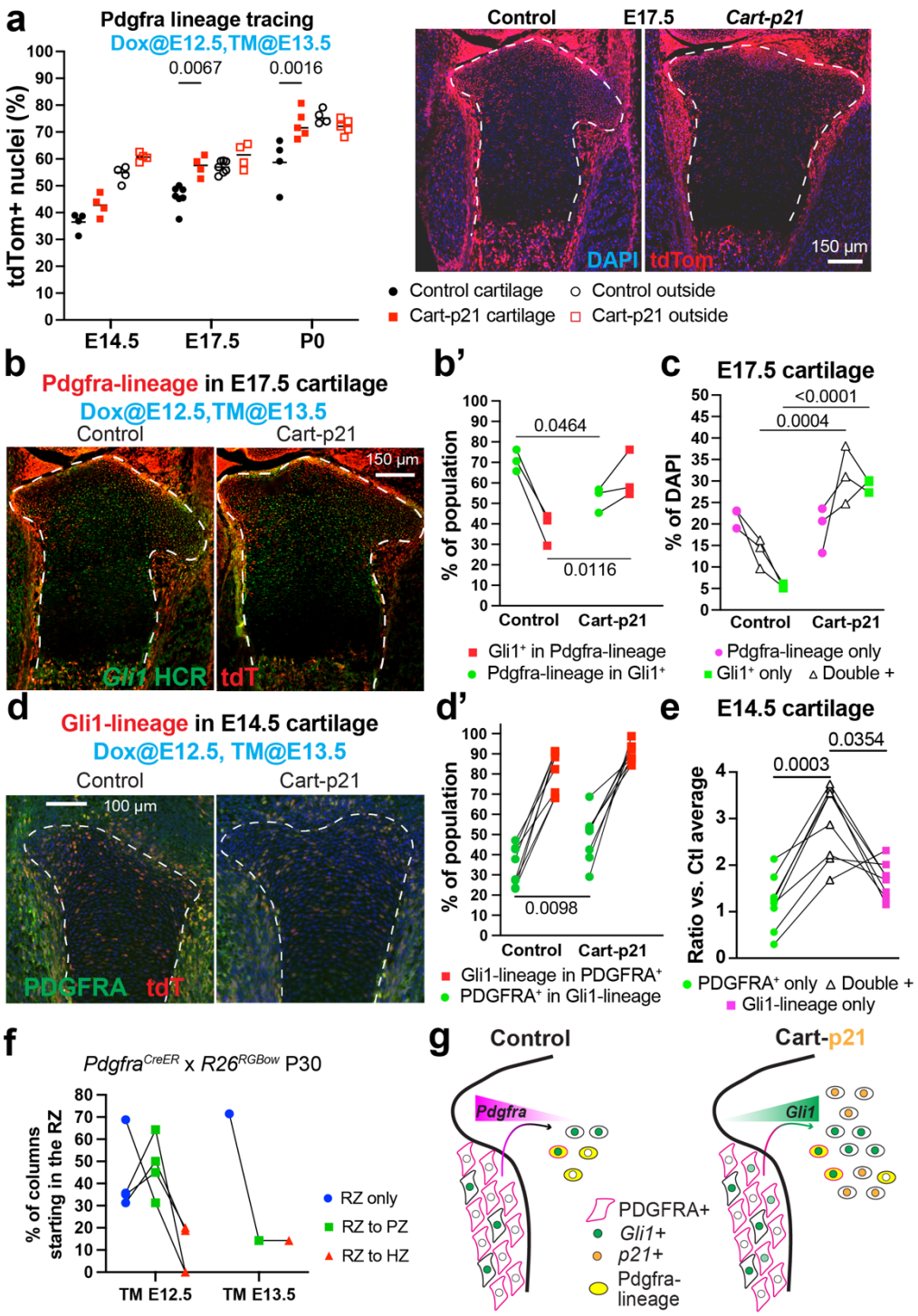

285

Figure 6. The contribution of the Pdgfra lineage to Gli1$^+$ LLCPs increases upon cartilage challenge. **a**, The Pdgfra lineage was traced in the absence and presence of *Pan-Cart-p21^{MOE}*, both inside and outside the cartilage (dashed lines; n=4 Ctl, 4 Exp at E14.5; 6, 4 at E17.5; 4, 5 at P0). **b-c**, Representative images (b) and quantification (b', c) of Pdgfra-lineage$^+$ and/or Gli1$^+$ cells in the E17.5 cartilage (n=3 Ctl, 3 Exp). **d-d'**, Representative images (d) and quantification (d') of Gli1-lineage$^+$ and/or PDGFRA$^+$ cells in the E14.5 cartilage (n=5 Ctl, 6 Exp). **e**, Ratio of the number of PDGFRA$^+$ and/or Gli1-lineage$^+$ cells in experimental cartilage, divided over the average of the same measurement in control samples. **f**, RGBow-expression was induced in Pdgfra$^+$ cells at either E12.5 (n=4) or E13.5 (n=1) and followed till P30. RZ, PZ, HZ: resting, proliferative, hypertrophic zone. The % of columns starting from RZ are shown, based on where they end. In a, b', c, d', e, p-values for Sidak's posthoc test after 2-way ANOVA. **g**, Potential model of how Pdgfra-lineage moving into the cartilage could become Gli1$^+$ LLCPs in response to *Pan-Cart-p21^{MOE}*.

286 *CCN2 impairs Gli1 expression and proliferation in chondrocytes, and is downregulated in Cart-p21*
287 *samples*

288 To determine how the *Pan-Cart-p21*^{MOE} challenge triggers *Gli1* upregulation, we performed another
289 transcriptomic approach, but this time shortly after challenge induction, separating Gli1-lineage and non-
290 Gli1-lineage cells (Ext. Data Fig. 8a). Pregnant females carrying *Gli1*$^{CreER/+}$*; R26*$^{LSL\text{-}tdTom/+}$*; Tigre*$^{TRE\text{-}p21/+}$
291 embryos (with or without *Col2a1-rtTA*) were provided with Dox at E12.5 and TM at E13.5, and embryos
292 were collected at E14.5. The whole hindlimb was processed for single-cell isolation and 10x Chromium
293 library preparation, multiplexed by sex (n=4 Exp and 4 Ctl samples, limbs from 2-3 embryos were pooled
294 per sample, see Online Methods). Coarse clustering was initially generated and further curated refined
295 manually (Ext. Data Fig. 8b, b'). Interestingly, in the coarse clustering, the two resting chondrocyte
296 subpopulations formed a continuum with the cells showing markers of the perichondrial groove of
297 Ranvier, a niche that hosts cells that can make contribution to cartilage[6], supporting the connection
298 between perichondrium and cartilage lineages. To identify gene signatures changed in *Cart-p21* limbs,
299 we performed pseudobulk differential gene expression analysis–which minimises false discovery
300 rates[24]–via edgeR (Ext. Data Fig. 8c). Besides the expected cell-cycle related genes (e.g. histone-
301 encoding), we noticed changes in genes related with chondrocyte activity and response to stress, such as
302 *cellular communication network factor 2* (*Ccn2*), also known as *connective tissue growth factor*[25-27],
303 which was downregulated in *Pan-Cart-p21*^{MOE} limbs (see Violin plot and Gene Ontology analysis in
304 Ext. Data Fig. 8c, d). We complemented these results by analysing cell-cell communication via
305 MultiNicheNet[28] in the E16.5 snRNA-seq and E14.5 scRNA-seq datasets. In all cases, *Ccn2*-mediated
306 communication was significantly downregulated in experimental samples (Ext. Data Fig. 8e-f'). We
307 confirmed this using *Ccn2* hybridisation chain reaction (HCR) on *Left-Cart-p21*^{MOE}, *Pan-Cart-p21*^{MOE}
308 and control samples (Fig. 7b, b', Ext. Data Fig. 8g, g'). These results were interesting considering our
309 previous study in which we showed that overexpression of *Ccn2* in the left cartilage (*Pitx2-Cre/+;*
310 *Col2a1-tTA/+; Tigre*$^{Dragon\text{-}Ccn2/+}$ model, Ext. Data Fig. 9a) impairs bone growth[15]. Using archival
311 samples of this model, we observed that the left hypertrophic zone was extremely reduced in size (Ext.
312 Data Fig. 9a'), and that proliferation in the resting zone (Ki67^{+} cells) was significantly downregulated
313 in the left cartilage as compared to the right one or control littermates (Ext. Data Fig. 9b, b').

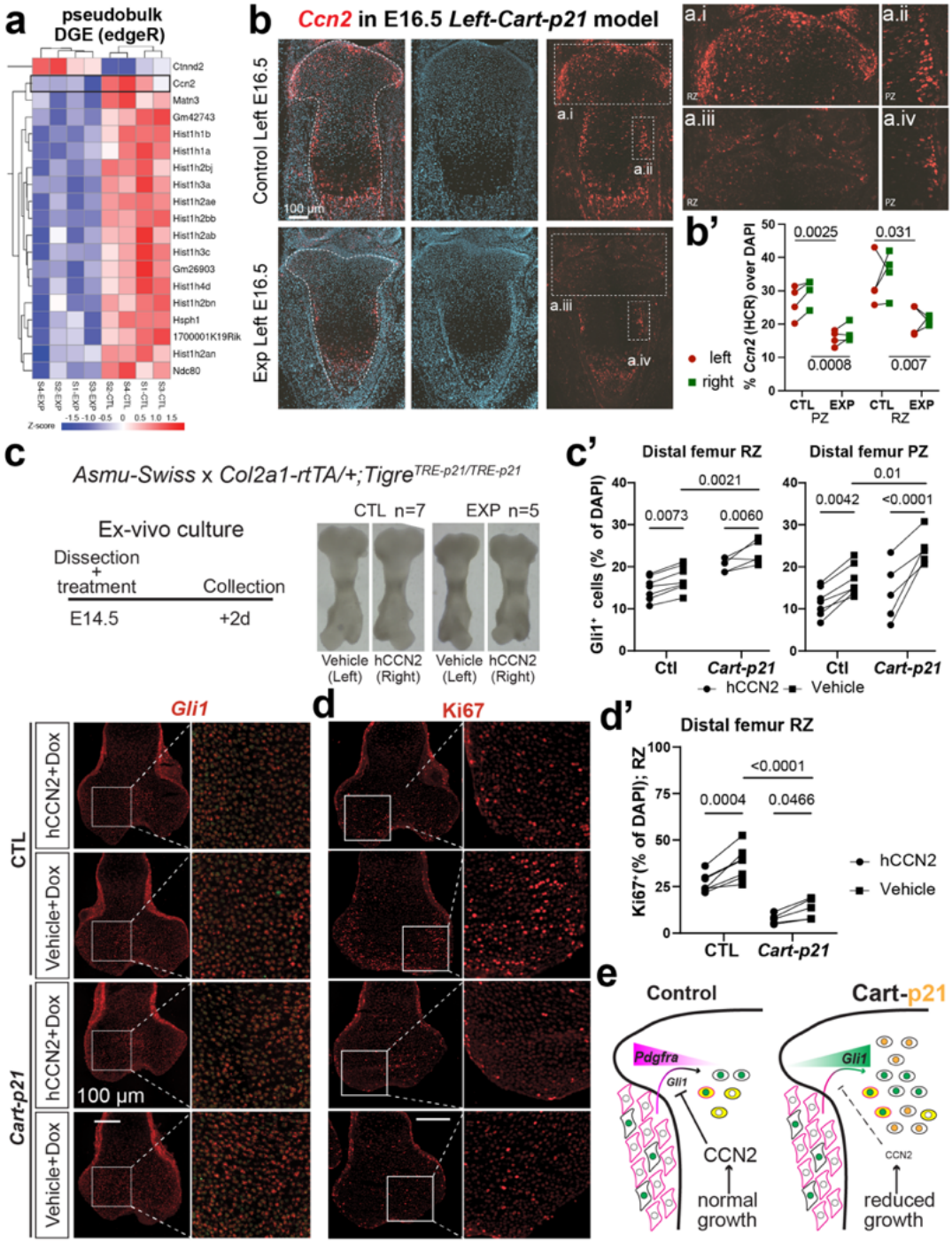

Figure 7. CCN2 impairs *Gli1* expression and proliferation in chondrocytes, and is downregulated in *Cart-p21^{MOE}* samples. a, Differential Gene Expression analysis (pseudobulk) of scRNA-seq data using edgeR. **b**, **b'**, *Ccn2* expression (HCR) in control and *Left-Cart-p21^{MOE}* E16.5 samples (a), as indicated, and quantified in (b). n=4 CTL and 4 EXP embryos. Boxed regions are shown magnified in b.i-iv. **c-d'**, Ex vivo culture procedure and representative images of *Gli1* (c) or Ki67 (d) staining and quantification (c' and d') in the indicated zones. n= 7 CTL, 5 EXP. Boxed regions are shown magnified on the sides. **e**, Proposed model of how CCN2 produced in specific cartilage zones limits *Gli1* expression in Pdgfra-derived chondrocytes during normal growth, whereas reduced CCN2 levels due to impaired growth in *Pan-Cart-p21^{MOE}* limbs leads to unrestricted *Gli1* activation in this population, so that some of them become LLCPs.

320 Given the results above, and that CCN2 has been proposed to orchestrate various signalling pathways to
321 promote harmonized skeletal growth[29], we hypothesised that CCN2 interferes with *Gli1* activation in
322 CPs, so that downregulation of *Ccn2* is what allowed the expansion of Gli1^{+} cells in the *Pan-Cart-*
323 *p21^{MOE}* models. To test this possibility, we cultured fetal femurs of control and *Pan-Cart-p21^{MOE}* fetuses
324 ex vivo (see Online methods) and treated them with human CCN2 (right femur from each embryo) or
325 Vehicle (left femur from each embryo) for ~2d (Fig. 7c). As predicted, *Gli1* expression was found
326 downregulated in treated samples–both Ctl and *Pan-Cart-p21^{MOE}*–(Fig. 7c'). Moreover, Ki67
327 immunostaining was used to detect proliferative cells, which were found to be diminished in treated
328 samples (Fig. 7d, d'). In summary, we concluded that the expansion of the Gli1-lineage, and the
329 compensatory proliferation triggered by cartilage cell-cycle arrest, were in part due to decreased CCN2
330 levels.

331 **Discussion**

332 Elucidating the origin and regulation of the LLCPs is crucial to understanding the evolution of limb size
333 and proportions, the factors that influence human height and the potential causes and treatments of
334 skeletal dysplasias. In mice, postnatal CPs have been described that can self-renew and give rise to long
335 columns of chondrocytes for most or the whole growth period[20,30,31]. However, given that at fetal and
336 perinatal stages only short columns are generated[7], it was unclear whether LLCPs are already present
337 (albeit inactive) in the early cartilage, or they are formed later. In either case, we hypothesised that the
338 system likely evolved with built-in robustness, such that transient developmental challenges may reveal
339 regulatory details of the process. Following this approach, we found that fetal Gli1-derived chondrocytes
340 expand in response to cell-cycle arrest in the cartilage and are required to compensate for this challenge
341 (Figs. 1, 2). We further found that Gli1^{+} cells give rise to LLCPs during normal growth (Fig. 3).
342 However, while we showed that the early cartilage anlage already contains Gli1^{+} quiescent CPs, our
343 results also suggested that Gli1^{+} cells outside the initial cartilage anlagen contribute to the LLCP pool
344 later, at least until birth (Fig. 4). Of note, chondrocytes arising from the Gli1-lineage in the last
345 gestational week were shown to be critical for acquiring normal bone length in the hindlimb (Fig. 5).
346 However, while bone length was significantly affected when Gli1-derived chondrocytes were ablated,
347 the effect was somewhat mild. This was probably due to compensation after Dox clearance. While we
348 tried to test this possibility by providing Dox postnatally, the rtTA that we used in our models did not
349 get sufficiently activated.

350 Interestingly, our single-cell RNA-seq analyses identified a continuous cluster including two resting
351 chondrocyte populations and one of cells expressing markers of the groove of Ranvier (Ext. Data Fig.

352 8b), with one of the resting populations within the Gli1^{high} subset being expanded at the expense of the
353 groove-of-Ranvier one (Ext. Data Fig. 10). It is important to note, however, that this approach is limited
354 because the Gli1 lineage had to be separated by FACS instead of bioinformatically identified, because
355 in the 10x approach, which is 3' biased, both the tdTom and the p21 transgenes yield reads mapping
356 mostly to WPRE, the RNA-stabilising sequence used in both alleles (Fig. 1b).

357 As per the origin of the Gli1^{+} CPs, our results suggested that some chondrocytes derive from stromal
358 Pdgfra^{+} cells (Fig. 6) revealing a previously unknown source of chondrocytes. Moreover, we showed
359 that these Pdgfra^{+} cells do not give rise to Gli1^{+} LLCPs during normal growth, but that they can become
360 *Gli1*$^{+}$ (and maintain PDGFRA expression at least briefly) in response to cartilage challenge. It remains
361 to be determined whether there is a chemoattractant signal emanating from the cartilage, capable of
362 recruiting Pdgfra^{+} cells. Such a signal could have therapeutic potential if it could be exogenously
363 provided to stimulate CP formation in situ, in a minimally invasive manner. In summary, our data
364 supports a model in which external cells always contribute to the cartilage, but mostly forming short-
365 lived CPs, unless they switch their behaviour in response to a growth challenge.

366 Lastly, regarding the signalling changes operating in the challenged limbs, differential gene expression
367 and cell-cell communication analyses showed that CCN2 levels were decreased in response to cartilage
368 cell-cycle arrest (Fig. 7). Intriguingly, *Ccn2* downregulation also happened in the right limbs of the *Left-*
369 *Cart-p21*^{MOE} model (Fig. 7b, Ext. Data Fig. 8f). Since we have previously shown that both left and right
370 limbs are equally affected in length in the *Left-Cart-p21*^{MOE} model[11], we propose that CCN2 levels
371 correlate with the overall growth output during fetal bone growth. Moreover, here we showed that excess
372 CCN2 impairs *Gli1* expression, chondrocyte proliferation and growth plate cytoarchitecture (Fig. 7 and
373 Ext. Data Fig. 9), leading us to propose a model in which CCN2 acts as a negative feedback signal (Fig.
374 7e). In this model, CCN2 levels reflect the growth status of the cartilage, such that reduced growth output
375 leads to decreased CCN2 and thus increased number of Gli1^{+} CPs, therefore unleashing long-term bone
376 growth potential. One limitation of this model is that *Gli1* upregulation was mostly detected in the ExpL
377 limb (Fig. 1a'), suggesting that CCN2 downregulation is necessary but not sufficient to derepress *Gli1*
378 expression. Future studies will focus on elucidating additional factors that could be used to convert
379 stromal cells in Gli1^{+} LLCPs, which could provide new avenues to stimulate cartilage regeneration in
380 situ.

381

382 **Methods**

383 *Animal models*

384 The use of animals in this study was approved by the Monash Animal Research Platform animal ethics
385 committee at Monash University.

386 Unilateral p21 misexpression model: The *Pitx2-ASE-Cre* (aka *Pitx2-Cre*) mouse line, obtained from
387 Prof. Hamada[9], was crossed with the *Col2a1-rtTA* mouse line[10], and then inter-crossed to generate
388 *Pitx2-Cre/Cre; Col2a1-rtTA* mice. In some experiments, a *Col2a1-eCFP* allele[32] was also included (a
389 kind gift from David Rowe). Genotyping was performed as described previously[11]. The $Tigre^{Dragon\text{-}p21}$
390 mouse line was previously described[11,15]. Experimental and control animals were generated by crossing
391 *Pitx2-Cre/Cre; Col2a1-rtTA/+* females with $Tigre^{Dragon\text{-}p21/Dragon\text{-}p21}$ males (i.e. homozygous for the
392 conditional misexpression allele). The separation of control and experimental animals was based on
393 the rtTA genotype. Pregnant females were administered doxycycline hyclate (Sigma) in water (1 mg/kg
394 with 0.5% sucrose for palatability) from E12.5 until collection (or until birth). The day of vaginal plug
395 detection was designated as E0.5, and E19.5 was referred to as P0.

396 Multi-colour lineage tracing: $Gli1^{CreER/CreER}$ female mice were time-mated with $R26R^{RGBow/RGBow}$ male
397 mice. The day of vaginal plug detection was referred to as E0.5, and E19.5 as P0. Pregnant females
398 were administered Tamoxifen (Sigma, stock at 20 mg/ml in corn oil) by oral gavage (180 µg/g) at
399 E12.5 (Experiment1) or E13.5 (Experiment2). Mouse embryos were collected at E14.5, E16.5, P0, P1,
400 P14, P30 (Experiment1) or E14.5,E15.5, E17.5,P0,P1,P14,P30 (Experiment2). Limbs were dissected
401 and fixed in 4% paraformaldehyde for 2d at 4ºC. Decalcification was performed on P14-P30 samples
402 by immersing them in 0.45M ethylenediaminetetraacetic acid (EDTA) in PBS from 10-14 days at 4ºC.

403 Pulse of nuclear GFP expression in cartilage: $Gli1^{CreER/CreER}$; $Tigre^{TRE\text{-}nGL/TRE\text{-}nGL}$ female mice were
404 time-mated with *Col2a1-rtTA/+*; $R26^{LSL\text{-}tdTom/LSL\text{-}tdTom}$ male mice. Experimental set 1: Pregnant females
405 were administered Dox in drinking water and Dox food (Specialty feeds SF08-026, 600mg/Kg) from
406 E12.5-E13.5. Tamoxifen was administered by oral gavage (180µg/g) at E13.5. Mouse embryos were
407 collected at E14.5,E17.5,P0,P14,P21. Experimental set 2: like set 1, except that Dox was given from
408 E17.5-E18.5, and offspring was collected at P0, P14,P21 and P30. Experimental set 3: Like set 2,
409 except that Dox was given from E12.5-E18.5, and offspring collected at P14. Limbs processed as
410 above.

411 Lineage tracing combined with p21 expression in all cartilage elements: $Gli1^{CreER/CreER}$ females[33] were
412 crossed with *Col2a1-rtTA/+*; $Tigre^{TRE\text{-}p21/TRE\text{-}p21}$; $R26^{LSL\text{-}tdT/LSL\text{-}tdT}$ males (described in [15,17]). Pregnant

413 females were given Dox food and water, plus tamoxifen (180 µg/g orally), at the stages described in
414 the main text. To trace other lineages, *Pdgfra*^{CreER} females[23] (a kind gift from Brigid Hogan) were used
415 instead of *Gli1*^{CreER} ones (tamoxifen 100 µg/g). *Pdgfra*$^{H2B\text{-}EGFP}$ mice[34] were a gift from Philippe
416 Soriano.

417 Unilateral *Ccn2* misexpression model: The *Pitx2-Cre* mouse line was crossed with the *Col2a1-tTA* one
418 that we previously described[11], and then inter-crossed to generate *Pitx2-Cre/Cre; Col2a1-tTA* mice.
419 The *Tigre*$^{Dragon\text{-}Ccn2}$ mouse line was previously described[15]. Experimental and control animals were
420 generated by crossing *Pitx2-Cre/Cre; Col2a1-tTA/+* females with *Tigre*$^{Dragon\text{-}Ccn2/Dragon\text{-}Ccn2}$ males (i.e.
421 homozygous for the conditional misexpression allele). The separation of control and experimental
422 animals was based on the tTA genotype. Pregnant females were not given Doxycycline, to allow for
423 tTA activity from the onset of chondrogenesis.

424 Generation of G4 mouse embryonic stem cells with Tigre docking site: a TIGRE docking site targeting
425 vector (a gift from Hongkui Zeng via Addgene plasmid #61580; http://n2t.net/addgene:61580;
426 RRID:Addgene_61580) was electroporated by Monash Genome Modification Platform into G4
427 mESCs (a gift from Andras Nagy) to generate an ESC line (MG36) with a docking site in the *Tigre*
428 (*Igs7*) locus, amenable for Flp-mediated cassette exchange. 192 individual clones were picked after 6
429 days of G418 selection. Out of the 96 analysed clones, 21 were positive by Southern hybridisation with
430 both 5' and 3' probes. After reanimation, these clones were analysed again by Southern hybridisation,
431 8 positive clones were further characterised by Southern hybridisation using internal neo probe (3
432 restriction digestions); 7 clones (#9, 13, 17, 32, 56, 61, 62) showed single integration. After sequencing,
433 all positive clones were found to have the correct sequence at F5 and F3 mutant FRT sites. 4 clones
434 were karyotyped: clones #56 and 62 are 100% euploid metaphase, whereas clone#32 was 87% euploid,
435 and clone#9 80% euploid.

436 Generation of *Tigre*$^{TRE\text{-}nucGreenLantern}$: AR157 vector, containing a TRE-H2B-GreenLantern and a PGK-
437 Hygro resistance split gene (N-half) flanked by FRT sites was generated by VectorBuilder (Exp Data
438 Fig. 6a). The vector also contained a Polylox cassette[35] downstream of the GreenLantern, but this
439 feature was not used in this study. This vector was then used by Monash Genome Modification
440 Platform for Flp-mediated cassette exchange (Exp Data Fig. 6a) into clones #56, 62 and 32 of *Igs7*-
441 targeted G4 ES cells (MG36, see above). 30µg pCAG-FlpO-IRES-Puro + 10µg AR157, mixed with
442 0.8ml of ESC suspension at ~1x10^{7}/ml and transferred to a 4mm cuvette. After incubation at RT for 5
443 min, electroporated by applying a single pulse (an exponential decay pulse at 250V, 500µF capacitance
444 or a square wave pulse at 250V, 5ms duration) followed by 5min at RT, then added into a 10-cm dish

445 pre-coated with MEFs. Two electroporation (one exponential decay pulse and one square wave pulse)
446 per clone was performed. 1 day after transfection, transfection efficiency was checked under the
447 fluorescent microscope, and drug selection was started (150µg/ml hygromycin). At 4 days after
448 transfection, selection was changed to hygromycin 100µg/ml. At 6 days after transfection, we picked
449 up 4 clones from each parental clone (#56-1 to 4, #62-1 to 4, #32-1 to 4) to MEF-coated 24-well plates.
450 These clones were genotyped by 5'- GT PCR, 3'- GT PCR and TRE-GL specific PCR (see below). All
451 clones were correctly targeted (Ext. Data Fig. 6b).
452

ES1 5'-GT PCR (245bp) 64ºC	
MG36 5'-GT step2 up	CGACCTCTAGAAGTAAGCTTTGAGC
MG36 5'-GT step2 down	CCTCCCCTGGCACAACGTAA
ES1 3'-GT PCR (449 bp) 64ºC	
MG36 3'-GT step2 up	ATCTTAGCCAGACGAGCGGG
MG36 3'-GT step2 down	AATGACCGCTGTTATGCGGC
TRE-GL GT PCR (448 bp) 62ºC	
TRE-GL GT up	GTGAACCGTCAGATCGCCTG
TRE-GL GT down	TGGATCCTTAGCGCTGGTGT

453
454 Clones #62-1, 62-2, 56-1 and 56-2 were used for two sessions each of blastocyst microinjection.
455 Males ET6 (clone 62-1, 85% chimera), ET28 (clone 62-2, 85% chimera), ET51 (clone #56-1, 80%
456 chimera), ET59 (clone #56-2, 80% chimera) were selected for breeding to next generation. One of
457 these lines was crossed with *Gli1*^{CreER} animals to establish the *Gli1*^{CreER}; *Tigre*$^{TRE\text{-}nGL}$ lines. Six
458 additional highly chimeric males were kept as back-up breeders.

459 *X-gal staining*

460 For enzymatic detection of β-galactosidase activity, the frozen sections were postfixed 5 min with 4%
461 paraformaldehyde (PFA, Electron Microscopy Sciences) in PBS at RT. After PBS washes, the sections
462 were incubated 2 x 5 min with X-gal buffer (2 mM $MgCl_2$, 0.02% NP40 and 0.05% deoxycholate in
463 PBS 0.1 M pH 7.4) and then overnight at 37ºC in X-gal reaction buffer (20 mg/ml X-gal, 5 mM
464 $K_4Fe(CN)_6$ and 5 mM $K_3Fe(CN)_6$ in X-gal wash buffer). After PBS rinses, the sections were postfixed
465 10 min in 4% PFA and PBS-rinsed again. The sections were then counterstained with Nuclear Fast

466 Red 0.005% for 15 min, serially dehydrated, incubated 3 x 1 min with xylene, and cover-slipped using
467 DPX mountant (Fisher).

468 *Single-nuclei and single-cell RNA-seq and analysis*

469 Single-nuclei RNA sequencing of unilateral p21 model

470 *Pitx2-Cre/Cre; Col2a1-rtTA/+; Col2a1-eCFP/+* females were crossed with *Tigre*$^{Dragon\text{-}p21/Dragon\text{-}p21}$
471 males and given Dox (1mg/ml in drinking water with 0.5% sucrose) at E12.5. The knee region
472 (obtained via orthogonal cuts from the hypertrophic region of the distal femur to the hypertrophic
473 region of the proximal tibia in skinned hindlimbs) of E16.5 Left and Right limbs from uCtl and *Left-*
474 *Cart-p21*^{MOE} samples (2 embryos of each genotype) were collected in DMEM with 10% DMSO and
475 5% calf serum, stored in a MrFrosty (ThermoFisher) at 4ºC for 10 min and then transferred to -80ºC
476 overnight. Tissue lysis and nuclei isolation were done as described by L.G.M. in
477 https://www.protocols.io/view/frankenstein-protocol-for-nuclei-isolation-from-f-5jyl8nx98l2w/v2, in
478 two batches of four samples each (left and right knees from one control and one experimental embryo).
479 Once ~5,000 nuclei per sample were collected, we proceeded immediately with the 10x Genomics
480 Single Cell Protocol (https://www.10xgenomics.com/support/single-cell-gene-
481 expression/documentation/steps/library-prep/chromium-single-cell-3-reagent-kits-user-guide-v-3-1-
482 chemistry, minimizing the time between nuclei preparation/sorting and chip loading. One chip per
483 batch was used (4 channels in each case, to load left and right samples from one control and one
484 experimental embryo). The libraries were sequenced twice on Novaseq (800 million clusters/read pairs
485 each time, which when combined amounted to ~40,000 reads per nuclei across the 8 samples).
486 Following sequencing, fastq reads were mapped against a custom reference that combined Mus
487 musculus (GRCm38) with transgenic genes (tdTomato, ECFP, and WPRE) using CellRanger
488 (v7.1.0). The resulting aligned reads were analysed via R (4.0.2). Seurat (v.4.2.1) and
489 R/Bioconductor SingleCellExperiment packages were used to generate count matrices. For each
490 sample, the mean of unique molecular identifiers (UMIs) (nCounts) was calculated and used as a
491 threshold to exclude empty droplets. Filtering was manually done according to the nCount and
492 number of genes. DoubletFinder (v2.0.3) was used to remove the expected doublets in each sample.
493 Harmony R package (v0.1.0) was also used to mitigate remove batch effects, and subsequently the
494 data were consolidated into a single Seurat object.
495 To identify the appropriate resolution, Clustree v 0.5.0 and Cluster Correlation analysis were used.
496 Visual representation of cluster assignments for individual cells was achieved within a reduced-
497 dimensional space using UMAP. To pinpoint the differentiation marker genes in the specific cluster

498 as compared to the remaining clusters, Wilcoxon Rank-Sum Test was used. This analysis was
499 conducted using the "FindAllMarkers" function within Seurat (v.4.2.1), p-value of less than 0.05 and
500 only.pos = T, and a log-fold change threshold of 0.1. To identify the cell type annotation, the clusters
501 were mapped with published mouse single cell hindlimb data[36]. In addition, previously reported
502 cellular biomarkers and Gene Ontology (GO) annotations were utilized to annotate the cell clusters.
503 The top 100 marker genes were utilized to enrich Gene Ontology (GO) terms through the
504 ClusterProfiler package (version 3.14.3). To identify and confirm the cell type, GSEA comparison
505 was also performed using SCP package (V. 0.5.1).

506 *Single Cell RNA-sequencing*

507 Sample preparation, collection, and sequencing: Female *Gli1*$^{CreER/CreER}$ mouse was crossed with
508 *Col2a1-rtTA; Tigre*$^{TRE-p21/TRE-p21}$; *R26*$^{LSL-tdT/LSL-tdT}$ male. At E12.5, the pregnant mouse was
509 administered by doxycycline in water (1 mg/ml with 0.5% sucrose) and food, and Tamoxifen was
510 orally gavaged (120 µg/g) at E13.5. At E14.5, the embryos were carefully dissected. Initially, the sex
511 and rtTA genotyping were determined using PCR-based quick genotyping and hindlimbs were then
512 meticulously dissected.
513 Afterwards, the tissue underwent treatment with Accumax in a rocker at 31ºC for 25 minutes (Ext.
514 Data Fig. 3a) and every 10 min, the samples were gently shaken. The supernatant was carefully
515 transferred into a tube and placed on ice for preservation, while the cartilaginous portions were exposed
516 to Collagenase B (5 mg/ml; Sigma) for ~90 min at 37ºC in a water bath (pipetted every 20 min). To
517 stop collagenase activity, we then added 700 µl of cold DMEM+20% FBS for each tube. We then
518 incorporated outer and inner supernatants, and the samples were resuspended in 20 volumes of 1x RBC
519 lysis buffer (including NH_4Cl, $NaHCO_3$, and EDTA) and incubated for 10 min RT on a rocker. The
520 cells were then centrifuged at 500 xg for 5 min at 4ºC and the cell pellet was then suspended in 900 µl
521 of PBS + 0.05% BSA. After re-washing, and the cells were resuspended in 400 ul of PBS + 0.05%
522 BSA. At the end, the cell suspension was filtered through 40-µm Flowmi® Cell Strainers and cells
523 were stained with DAPI (0.05 µg/ml) and transferred into Falcon™ Round-Bottom Polypropylene
524 (Fisher Scientific). The tdT+ and tdT- cells were sorted using flow cytometry (nozzle size of 100 µm,
525 operating at a PSI of 20 and a BOP of 223).
526 In total, two experimental males, two control males, two control females, and only one experimental
527 female were utilized. The cells were counted by an automated cell counter (ThermoFisher) using trypan
528 blue staining and all passed at least 90% cell viability. Then, the cell suspensions were centrifuged at
529 500 xg for 5 min at 4ºC to decrease the final volume. The samples (S) were then multiplexed based on

530 sex and conditions. Specifically, for S1, EM^{tdt+} (Experimental Male) and CF^{tdt+} (Control Female) cells
531 were multiplexed, totalling 7,500 cells. For S2, EM^{tdt-} and CF^{tdt-} cells were multiplexed, amounting to
532 25,000 cells (at a concentration of 1000 cells/µl with a volume of 25 µl). In S3, EF^{tdt+} and CM^{tdt+} cells
533 were multiplexed, totalling 5,700 cells. Finally, in S4, EF^{tdt-} and CM^{tdt-} cells were multiplexed,
534 comprising 24,000 cells. After that, the process was carried out according to the 10X Genomics
535 protocol (https://www.10xgenomics.com/support/single-cell-gene-
536 expression/documentation/steps/sample-prep/single-cell-protocols-cell-preparation-guide).
537 The libraries were prepared using Chromium Next GEM Single Cell 3' Reagent Kits v3.1 (10X
538 Genomics) according to manufacturer's directions and then sequenced on Illumina (~833 million
539 clusters/read pairs each time) with a length of 100 bp. All samples were passed the quality of cDNA
540 (refer to the GSE File).

541 scRNA-seq preprocessing: The fastq files were aligned against a custom reference comprising *Mus*
542 *musculus* (GRCm38; obtained from 10X Genomics Ref.) along with transgenic genes (tdTom,
543 $CreER^{T2}$, and WPRE) using CellRanger (v7.2.0). In total, more than 98.2% of Reads Mapped to
544 Genome and 25,190 genes were detected as well as transgenes. To eliminate contaminated cells with
545 ambient RNA, CellBender V 0.3.0 was used. The expected number of genuine cells and total droplets
546 were estimated based on the CellRanger output, using the Raw_feature_bc_matrix.h5 file as input.
547 Identified unique molecular identifiers (UMIs) were then mapped and subset from the Seurat object
548 generated by the filtered feature barcode matrix file. DoubletFinder (v2.0.3)[37] was then used to remove
549 expected doublets in each sample, with pK calculated separately for each sample. Then the cells with
550 low nCount_RNA and nFeature_RNA were filtered out.

551 Testing for differences in cell type proportions: To analyse the distinct cellular compositions among
552 conditions, the propeller test available in the speckle R (v.0.0.1, accessible at
553 https://github.com/Oshlack/speckle) was employed. The groups were classified with a false discovery
554 rate (FDR) of ≤0.1 as indicative of notable variations in cell types.

555 MultiNicheNet: To investigate cell-to-cell communication, MultipleNichenetR (version 1.0.0)[38] was
556 used. The Seurat object was first converted to a SingleCellExperiment (SCE), and all genes were
557 mapped using the alias_to_symbol_SCE function to "mouse." A cutoff point of min_cells = 10 was
558 used, and differentially expressed genes were calculated using the get_DE_info function. The
559 following parameters were applied: logFC_threshold = 0.5, p_val_threshold = 0.05, fraction_cutoff =
560 0.05, and empirical_pval = TRUE. To achieve more robust results and minimize cluster dropouts
561 caused by low number of cells, some subclusters were merged. Ligand-receptor interactions were

562 identified via the "multi_nichenet_analysis" function, and the results were visualized using
563 MultiNicheNetR's built-in functions[38].

564 SCENIC analysis: SCENIC (version 1.2.4)[39] was used to assess gene regulatory network activities in
565 each cell population. For snRNA-seq data, pySCENIC[40] was employed and then data manually
566 converted to SCENIC in R. A co-expression network was generated using the GENIE3 function, and
567 the Area Under the Curve (AUC) was calculated with AUCell. The AUC values were normalized to a
568 range of 0 to 1 for each regulon and regulon scores were obtained using the 'get_AUC' function. To
569 identify significant changes in regulon activity across conditions, t-tests and Wilcoxon tests were
570 conducted for each cluster in the relevant condition.

571 *EdU incorporation and detection*

572 A solution of 5-Ethynyl-2'-deoxyuridine (EdU) was prepared at 6 mg/ml in phosphate-buffered saline
573 (PBS). This solution was administered at a dose of 60 µg/g, subcutaneously (s.c) for pups and 30 µg/g
574 intraperitoneally (i.p.) for pregnant females, 1.5 hours before euthanizing the mice (or 2 days before,
575 for pulse-chase experiments). To detect EdU, a click chemistry reaction with fluorescein-conjugated
576 azide (Lumiprobe #A4130) was performed once the immunohistochemistry and/or TUNEL staining
577 were completed on the same slides. Briefly, the working solution was prepared in PBS, adding $CuSO_4$
578 (Sigma # C1297) to 4 mM, the azide to 0.4 µM and freshly-dissolved ascorbic acid (Sigma #A0278)
579 to 20 mg/ml, and incubating the sections for 15 min at room temperature in the dark, followed by PBS
580 washes.

581 *Sample collection and histological processing*

582 Mouse embryos were euthanized using hypothermia in cold PBS, while mouse pups were euthanized
583 by decapitation. Upon collection of the embryos or pups, the limbs (including full tibiae and/or femora)
584 were carefully dissected out in cold PBS, skinned, and fixed in 4% paraformaldehyde (PFA) for 2 days
585 at 4ºC. Samples of P1 or younger were not subjected to decalcification. For P3, P5, and P7 samples,
586 decalcification was performed by immersing the specimens in 0.45M ethylenediaminetetraacetic acid
587 (EDTA) in PBS for 3, 5, and 7 days, respectively, at 4ºC. Following several washes with PBS, the limb
588 tissues were cryoprotected in PBS containing 15% sucrose and then equilibrated in 30% sucrose at 4ºC
589 until they sank. The hindlimbs were then oriented sagittally, facing each other, with the tibiae
590 positioned at the bottom of the block (closest to the blade during sectioning) and embedded in Optimal
591 Cutting Temperature (OCT) compound using cryomolds (Tissue-Tek). The specimens were frozen by
592 immersing them in dry-ice-cold iso-pentane (Sigma). Serial sections with a thickness of 7 µm were

593 collected using a Leica Cryostat on Superfrost slides. The sections were allowed to dry for at least 30
594 minutes and stored at -80ºC until further use. Prior to conducting histological techniques, the frozen
595 slides were brought to room temperature in PBS, and the OCT compound was washed away with
596 additional rounds of PBS rinses.

597 *Ex vivo culture*

598 The culture medium was prepared by mixing 200 µL penicillin/streptomycin (10,000 U/mL) with 48.9
599 mL high-glucose DMEM, 500 µL Glucomax, 100 mg BSA, 2.5 mg ascorbic acid, and 400 µL β-
600 glycero-phosphate, then filtered through a 0.2 µm filter. E14.5 embryos were dissected and transferred
601 to pre-warmed media under a tissue culture hood. Each hindlimb was placed in cold Accumax and then
602 digested at 31ºC for at least 35 minutes. The samples were then put on ice, and the tibia and femur
603 were dissected individually. Limbs were cultured in 48-well plates with 500 µL of media at 37ºC in a
604 5% CO_2 incubator for approximately 2 hours before initiating treatment. For the treatment, human
605 recombinant CCN2 (Peprotech, 17840573) was used. One limb from each pair was treated with 100
606 ng/mL of CCN2 + Doxycycline, while another set received Doxycycline + Vehicle (1% BSA in
607 Saline). After 2 days, the limbs were treated with 10 µM EdU for 1h before fixation in PFA.

608 *Micro-CT and bone length analysis*

609 The micro-CT and bone length analysis was as previously described[41]. Briefly, samples were retained
610 and fixed in 4% PFA as residual tissues from other experiments in the Rosello-Diez lab. Whole femora
611 and humeri were scanned using a Siemens Inveon PET-SPECT-CT small animal scanner in CT
612 modality (Monash Biomedical Imaging). The scanning parameters included a resolution of 20 and 40
613 µm, 360 projections at 80 kV, 500 µA, 600 ms exposure with a 500 ms settling time between
614 projections. Binning was applied to adjust the resolution with 2 x 2 for 20 µm scans and 4 x 4 for 40
615 µm scans. The acquired data were reconstructed using a Feldkamp algorithm and converted to DICOM
616 files using Siemens software. For the analysis and bone length measurements, Mimics Research
617 software (v21.0; Materialize, Leuven, Belgium) equipped with the scripting module was utilized to
618 develop the analysis pipeline[41].

619 *Immunohistochemistry and TUNEL staining*

620 For antigen retrieval, the sections were subjected to citrate buffer (10 mM citric acid, 0.05% Tween 20
621 [pH 6.0]) at 90˚C for 15 minutes. Afterward, the sections were cooled down in an ice water bath,
622 washed with PBSTx (PBS containing 0.1% Triton X-100). To perform TUNEL staining, the
623 endogenous biotin was blocked using the Avidin/Biotin blocking kit (Vector #SP-2001) after antigen

624 retrieval. Subsequently, TdT enzyme and Biotin-16-dUTP (Sigma #3333566001 and #11093070910)
625 were used according to the manufacturer's instructions. Biotin-tagged DNA nicks were visualized using
626 Alexa488- or Alexa647-conjugated streptavidin (Molecular Probes, diluted 1/1000) during the
627 incubation with the secondary antibody.

628 For immunohistochemistry staining, sections were incubated with the primary antibodies prepared in
629 PBS for either 1.5 hours at room temperature or overnight at 4˚C (see list of antibodies below).
630 Following PBSTx washes, the sections were incubated with Alexa488-, Alexa555-, and/or Alexa647-
631 conjugated secondary antibodies (Molecular Probes; diluted 1/500 in PBSTx with DAPI) for 1 hour at
632 room temperature. After additional PBSTx washes, the slides were mounted using Fluoromount™
633 Aqueous Mounting Medium (Sigma). The antibodies used, along with their host species, vendors,
634 catalogue numbers, and dilutions, were as follows: mCherry (goat polyclonal, Origene Technologies
635 #AB0040-200, diluted 1/500), p-S6 (rabbit polyclonal, Cell Signaling Technology #2211S, diluted
636 1/300).

637 *In situ hybridization*

638 To perform *in situ* hybridisation, sections were fixed in 4% PFA for 20 minutes at room temperature,
639 washed in PBS, and treated with 4µg/ml Proteinase K for 15 minutes at 37ºC. After washing in PBS,
640 the sections were refixed with 4% PFA, followed by treatment with 0.1N pH8 triethanolamine (Sigma
641 #90279), 0.25% acetic anhydride (Sigma #320102) for 10 minutes at room temperature. Subsequently,
642 the sections were washed in PBS and water and incubated with prehybridization buffer (50%
643 formamide, 5x SSC pH 5.5, 0.1% 3-[(3-Cholamidopropyl)dimethylammonio]-1-propanesulfonate
644 (CHAPS), 0.05 mg/ml yeast tRNA, 0.1% Tween 20, 1x Denhardt's) at 60ºC for 30 minutes. The
645 sections were then incubated with 1µg/ml preheated riboprobes and subjected to hybridization at 60ºC
646 for 2 hours. Post-hybridization washes were performed using post-hybridisation buffer I (50%
647 formamide, 5x pH 5.5 SSC, 1% SDS) and II (50% formamide, 2x pH 5.5 SSC, 0.2% SDS) preheated
648 at 60ºC for 30 minutes, respectively. The sections were then washed with maleic acid buffer (MABT:
649 100mM maleic acid, 150mM NaCl, 70mM NaOH, 0.1% Tween 20) and blocked with 10% goat serum,
650 1% blocking reagent (Roche #11096176001) in MABT at room temperature for 30 minutes. Next, the
651 sections were incubated overnight at 4ºC with anti-digoxigenin-AP (Sigma #11093274910) diluted
652 1/4000 in MABT with 2% goat serum and 1% blocking reagent. After several MABT washes, the
653 sections underwent incubation with AP buffer (0.1M Tris-HCL pH 9.5, 0.1M NaCl, 0.05M $MgCl_2$,
654 0.1% Tween 20), with the second one containing 1mM levamisole and then developed colour using
655 BM purple (Roche #11442074001) at 37ºC. Following a wash in PBS, the sections were fixed for 10

656 minutes in 4% PFA, counterstained with Nuclear Fast Red (Sigma #N3020) at room temperature for
657 10 minutes, and rinsed in water. Dehydration was performed by passing the sections through 70%,
658 90% ethanol, absolute ethanol, and xylene. Finally, the sections were mounted with DPX (Sigma
659 #100579).

660 *Hybridisation chain reaction (HCR)*

661 Slides were thawed for 20 min in RNAse-free PBS (DPBS; GIBCO, Invitrogen, LOT: 866200), washed
662 twice with DPBS, and fixed in ice-cold 4% paraformaldehyde for 15 min at 4ºC. Samples were then
663 dehydrated in 50%, 75%, and 100% ethanol for 5 min each at room temperature. After washing with
664 DPBS, slides were placed in a pre-warmed humidified chamber, and 200 µL of probe hybridization
665 buffer was added for 10 min. Probes (95 µL, 16 nM) were then applied and incubated for > 12 hours
666 at 37ºC.

667 To remove excess probes, slides were washed sequentially with 75%, 50%, and 25% probe wash buffer
668 (24 mL formamide 100% with 20 mL 20x SSC, 1,440 µl of Citric acid 0.5 M, 80 µl Tween20, 200 µl
669 20 mg/mL heparin, and fill up to 80 mL with ultrapure water) in 5x SSCT, followed by 100% 5x SSCT,
670 each for 15 min, then immersed in 100% 5x SSCT for 5 min at room temperature. Amplification was
671 initiated by adding 200 µL of amplification buffer for 30 min at room temperature. Hairpins h1 and h2
672 (6 pmol each) were snap-cooled and mixed with amplification buffer. After removing the pre-
673 amplification solution, 98 µL of the hairpin solution was added, and slides were incubated for at least
674 12 hours in a dark, humidified chamber. Slides were washed twice with 5x SSCT for 30 min and once
675 for 5 min, then mounted with Fluoromount-G™ (Cat: 00495802, USA).

676 *Imaging*

677 Sagittal sections of the limbs were captured, with a focus on the area between the distal femora and
678 proximal tibiae. Typically, at least 2 sections per limb were analysed, although in most cases 4 sections
679 were examined. In the case of cultured distal femora, frontal sections were used as they provided better
680 identification of the different epiphyseal regions. To determine the boundaries of the resting zone (RZ),
681 proliferative zone (PZ) and hypertrophic zone (HZ), morphological criteria were applied. The transition
682 between round (resting) and flat (columnar) nuclei, forming an arch along the upper point of the
683 grooves of Ranvier, was considered as the start of the PZ. On the other hand, the transition towards
684 larger, more spaced nuclei (pre-hypertrophic) marked the end of the PZ. The point where the
685 pericellular matrix exhibited a sharp reduction around enlarging chondrocytes was designated as the
686 beginning of the HZ. The distal end of the last intact chondrocyte served as the endpoint of the HZ.

687 For imaging, bright-field and fluorescence images were acquired using a Zeiss inverted microscope
688 (Imager.Z1 or Z2) equipped with Axiovision software (Zeiss/ZenBlue). Mosaic pictures were
689 automatically generated by assembling individual tiles captured at 10x magnification for bright-field
690 images or 20x magnification for fluorescence images.

691 *Image analysis and quantification*

692 The regions of interest such as resting, proliferative and hypertrophic zones (RZ, PZ, HZ) and the
693 secondary ossification centre (SOC) were identified from imaged sections of the multiple models (left
694 and right; experimental and control proximal tibial cartilage). Consistent parameters such as brightness,
695 contrast, filters and layers were kept the same for all the images in the same study.

696 *Cell count analysis*

697 The RZ and PZ were identified and segmented from sections stained for DAPI, tdTomato, and TUNEL
698 or EdU using macros on FIJI software. Details of the macros are available upon request. The number
699 of cells in the region of interest (RZ & PZ) were measured using CellProfiler. Since in our hands
700 CellProfiler did not work properly with more than 3 channels, a pipeline was generated to split the four
701 channels into DAPI on one hand and the 3 other channels on the other hand. The two sets of images
702 were run on CellProfiler separately. The CellProfiler pipelines are also available upon request.

703 *Statistical analysis*

704 Statistical comparisons were performed using appropriate tests based on the experimental design. An
705 unpaired t test was used for comparisons involving one variable and two conditions. Two-way ANOVA
706 was utilized for comparisons involving two variables and two or more conditions. Non-parametric tests
707 were selected when the assumption of normality could not be met. All statistical analyses were
708 conducted using Prism10 software (GraphPad).

709

710 **Figure legends**

711 **Figure 1. Mosaic cell-cycle arrest in the fetal cartilage triggers compensation from Gli1$^+$ stromal**
712 **cells. a**, **a'**, A left-specific, cartilage-targeted p21 over-expression model (*Left-Cart-p21^{MOE}*) was used
713 for snRNA-seq analysis of knees. Left (L) and right (R) knees were processed separately but analysed
714 together in control embryos (a). Chondrocyte-related cells were analysed via SCENIC and relevant
715 regulons are shown boxed (a', dashed lines denote mild changes). **b**, **b'**, Expression of p21 in the
716 cartilage, induced from E12.5 to P0 (b), does not lead to growth defects (b'). The table shows results of
717 2-way ANOVA. **c**, **c'**, The Gli1 lineage was followed in absence (Control) and presence of p21
718 misexpression (*Pan-Cart-p21^{MOE}*), and quantified in the regions shown in (c). In c', data shown as
719 mean± SD. p-values for Sidak's multiple comparisons test after 2-way ANOVA are shown.

720 **Figure 2. Gli1-derived chondrocytes are needed for compensation of *Cart-p21*. a**, A *Dragon-aDTA*
721 allele was combined with *Gli1^{CreER}* and *Pan-Cart-p21^{MOE}* to ablate Gli1-derived chondrocytes during
722 p21-triggered compensation. **b, b'**, Representative images of TUNEL (b, cartilage outlined) and
723 quantification (b') in the indicated stages and genotypes (n=8,6,6 at E17.5, n=6,5,10 at P0). Significant
724 p-values for Tukey's test after ANOVA are shown. **c**, Length of the P0 mineralised region is shown for
725 the indicated genotypes as mean±SD (n=17, 9, 10). Significant p-values of Sidak's multiple comparisons
726 test (after 2-way ANOVA) are shown.

727 **Figure 3. Fetal Gli1$^+$ cells give rise to most chondrocytes in the juvenile and adult growth plate. a**,
728 Examples of Gli1-lineage tracing after TM induction at E12.5 or E13.5, analysed at the indicated stages.
729 **b**, Quantification of reporter-expressing cells, inside and outside the cartilage for TM-E12.5 (left,
730 n=6,5,6), or in cartilage for both inductions (right, n=4,2). **c-c''**, The tri-colour reporter RGBow was
731 used to quantify individual clones in the growth plate (c, added average of each colour is shown), at
732 multiple times post induction (n=3, 4, 3, 3, 3, 3 for TM-E12.5, n=3, 3, 2, 2, 2, 3, 3 for TM-E13.5). RZ,
733 PZ, HZ: resting, proliferative, hypertrophic zone. In c', the % of P30 columns starting from RZ are
734 shown, based on where they end (n= 3 and 4). c'' shows representative images **d**, number of cells per
735 RZ-rooted column, for the stages and induction times indicated.

736 **Figure 4. Most fetal LLCPs belong to the Gli1 lineage**. **a**, **a'**, Model to label the Gli1 lineage and
737 label-retaining chondrocytes (a) and a representative image of the distribution after early labelling (a').
738 **b-b''**, Quantification of single-positive and double-positive populations in the cartilage at the indicated
739 stages after induction at E12.5-E13.5 (b, n=3, 3, 4, 2), E17.5-E18.5 (b', n=4, 3, 3, 2) or E12.5-E18.5
740 (b'', n=4). *: quantified in resting zone only. **c**, Representative images of tdT and nGL overlap
741 (arrowheads) at P14 with 2 different induction regimes. SOC, secondary ossification centre (separated

742 from cartilage by dashed lines). **d-e''**, % of tdT^+ cells within the GL^+ population (d-d'') or GL^+ cells
743 within the tdT^+ population (e-e'') after 1-day Dox pulse at E12.5 (d, e) or E17.5 (d', e') or 6-day pulse
744 at E12.5 (d'', e''). In all graphs p-values for multiple comparisons tests after 2-way ANOVA are shown.
745 **Figure 5. a**, The *Dragon-aDTA* allele was combined with *Gli1*^{CreER} and *Col2a1-rtTA* to activate
746 diphtheria toxin expression exclusively in Gli1-lineage chondrocytes in the last week of gestation (*Gli-*
747 *Cart-DTA* model). **b**, **b'** Typical images (b) and quantification (b') of $TUNEL^+$ cells (arrowheads) at the
748 indicated stages. **c** Bone length of Ctl and *Gli-Cart-DTA* mice at postnatal day 100 (P100). In b' and c,
749 p-values of multiple comparisons tests after 2-way ANOVA are shown. RZ, PZ: resting proliferative
750 zone.

751 **Figure 6. The contribution of the Pdgfra lineage to $Gli1^+$ LLCPs increases upon cartilage**
752 **challenge**. **a**, The Pdgfra lineage was traced in the absence and presence of *Pan-Cart-p21*^{MOE}, both inside
753 and outside the cartilage (dashed lines; n=4 Ctl, 4 Exp at E14.5; 6, 4 at E17.5; 4, 5 at P0). **b-c**,
754 Representative images (b) and quantification (b', c) of Pdgfra-lineage$^+$ and/or $Gli1^+$ cells in the E17.5
755 cartilage (n=3 Ctl, 3 Exp). **d-e**, Representative images (d) and quantification (d', e) of Gli1-lineage$^+$
756 and/or $PDGFRA^+$ cells in the E14.5 cartilage (n=5 Ctl, 6 Exp). **f**, RGBow-expression was induced in
757 $Pdgfra^+$ cells at either E12.5 (n=4) or E13.5 (n=1) and followed till P30. RZ, PZ, HZ: resting,
758 proliferative, hypertrophic zone. The % of columns starting from RZ are shown, based on where they
759 end. In a, b', c, d', e, p-values for Sidak's posthoc test after 2-way ANOVA. **g**, Potential model of how
760 Pdgfra-lineage moving into the cartilage could become $Gli1^+$ LLCPs in response to *Pan-Cart-p21*^{MOE}.

761 **Figure 7. CCN2 impairs *Gli1* expression and proliferation in chondrocytes, and is downregulated**
762 **in *Cart-p21* samples. a**, Differential Gene Expression analysis (pseudobulk) of scRNA-seq data using
763 edgeR. **b**, **b'**, *Ccn2* expression (HCR) in control and *Left-Cart-p21*^{MOE} E16.5 samples (a), as indicated,
764 and quantified in (b). n=4 CTL and 4 EXP embryos. Boxed regions are shown magnified in a.i-iv. **c-d'**,
765 Ex vivo culture procedure and representative images of *Gli1* (c) or Ki67 (d) staining and quantification
766 (c' and d') in the indicated zones. n= 7 CTL, 5 EXP. Boxed regions are shown magnified on the sides.
767 **e**, Proposed model of how CCN2 produced in specific cartilage zones limits *Gli1* expression in Pdgfra-
768 derived chondrocytes during normal growth, whereas reduced CCN2 levels due to impaired growth in
769 *Pan-Cart-p21*^{MOE} limbs leads to unrestricted *Gli1* activation in this population, so that some of them
770 become LLCPs.
771
772

773 **Extended Data Figure legends**

774 **Extended Data Figure 1.** Possible origins of postnatal cartilage progenitors (CPs). **a**, Cartilage-resident
775 short-lived CPs eventually become long-lived, due to intrinsic and/or extrinsic triggers. **b**, Precursors of
776 long-lived CPs (Pre-LLCPs) already exist in the fetal limb as a separate population (in the cartilage
777 and/or outside), and only become active/recruited postnatally, in response to cartilage maturation. RZ,
778 PZ, HZ, resting, proliferative, hypertrophic zones; SOC, secondary ossification centre; PCh,
779 perichondrium.

780 **Extended Data Figure 2. a**, Double-conditional model for inducible and reversible gene
781 overexpression. TRE, Tetracycline-responsive element. WPRE, RNA stabilising sequence. **b**, Expected
782 accelerated depletion of chondroprogenitors in response to mosaic p21 expression. **c**, Minor to no
783 asymmetries are generated by P100 despite the overactivation of perinatal CPs**.**

784 **Extended Data Figure 3. a**, Schematic of the process for sample collection, processing of single-nuclei
785 RNA sequencing and quality control in Seurat processing. **b-b'**, Dotplot graph illustrating the markers
786 of each of the 32 initially identified clusters (b) and chondrocyte-related clusters only (b'). **c**, Heatmap
787 of average gene expression of all clusters showing the accuracy of clustering. **d-d'**, UMAP of all
788 identified clusters (d). The highly correlated clusters (lateral plate mesoderm-derived cells, LPM) are
789 shown boxed by black rectangles on the heatmap (c), and subclustered in (d'). **e-e'**, Gli1+ cells in the
790 LPM group (e) and distribution of LPM populations within Gli1^{+} cells in Ctl and Exp limbs (e'). *
791 denotes a significant difference identified by Propeller.

792 **Extended Data Figure 4. a**, **a'**, % of p21^{+} nuclei found in the proximal tibia cartilage of Cart-p21 mice
793 at the shown stages, with Dox at E12.5 (a) or E13.5 (a'). p-values of multiple-comparisons tests after
794 ANOVA are shown. **b**, The Gli1 lineage was followed in Control and Cart-p21 samples, and quantified
795 inside and outside the cartilage (defined in Fig. 4c). **c-c''**, Distribution of tdT^{+} cells in resting (RZ) and
796 proliferative zone (PZ) of Ctl and *Pan-Cart-p21^{MOE}* samples at E14.5 (c), E17.5 (c') and P0 (c''). **d**, **d'**,
797 Idem, for P0 samples with TM-E12.5 and Dox at E13.5 (d) or E12.5 (d'). In b-d', p-values for multiple
798 comparisons tests after 2-way ANOVA are shown.

799 **Extended Data Figure 5.** Expression of Gli1 (a, a') and Pdgfra (b, b') in the embryonic day (E)14.5
800 and postnatal day (P)1 hindlimb, as indicated. Fe, femur, Ti, tibia. Dashed lines delineate the cartilage.
801 Some images were taken from GenePaint (a, b).

802 **Extended Data Figure 6. a**, Targeting strategy to generate ES cell lines carrying a Tet-responsive
803 element (TRE)-controlled nuclear green lantern (H2B-GL) gene in the Tigre locus. Successful FlpO-

804 mediated cassette exchange reconstitutes the Hygro-resistance gene. SA, splice acceptor. pA, poly A.
805 Ins, insulator. FRT, flippase recognition target. WPRE, RNA-stabilising sequence from Woodchuck
806 virus. PGK, constitutive mammalian promoter. **b**, Confirmation of initially picked clones (left) and
807 subclones (right) by 5'/3'/TRE-GL specific PCR reactions. **c**, **c'**, Representative images (c) and
808 quantification in the yellow region of interest (c') of the single- and double-labelled cells, upon TM and
809 Dox induction, as indicated. **d**, Quantification of Ki67^{+} (i.e., cycling) cells, both GL^{+} and GL^{-}, in the
810 RZ. Stages and Dox treatment are indicated. p-values for multiple comparisons test after 2-way ANOVA
811 are shown.

812 **Extended Data Figure 7. a-b'**, Quantification of EdU in p21-negative chondrocytes of resting and
813 proliferative zones (a, b, as indicated) and in cells outside the cartilage (a', b'), at E14.5 (a-a') and E17.5
814 (b-b'), distinguishing between Pdgfra-lineage and non-lineage cells. In (a-b'), p-values for multiple
815 comparisons test after 2-way ANOVA are shown. **c-d'**, Tri-colour lineage tracing of Pdgfra^{+} cells, upon
816 TM injection at E12.5 (c, d, boxed region amplified in c') and E13.5 (d'). For the quantifications in d
817 and d', the average number of columns of each colour per sections was added up to obtain a total number
818 of columns per section per sample.

819 **Extended Data Figure 8. a**, Design of the lineage-specific single-cell RNA-seq approach, multiplexed
820 by sex. **b**, **b'**, Coarse (b) and fine (b') clustering outcome of the curated sequencing data (see Online
821 Methods). **c**, Violin plot showing expression of *Ccn2* in the different populations identified in the
822 scRNA-seq data, for the 2 genotypes. CTL= CTN+CTP, EXP= ETN+ETP. **d**, Gene Ontology terms
823 related to Ccn2, differentially enriched in EXP vs. CTL samples. **e-f'**, MultiNicheNet analysis of cell-
824 cell communication in Proliferating Chondrocytes of the snRNA-seq (e) and the scRNA-seq dataset (f),
825 as well as Resting chondrocytes of the scRNA-seq dataset (f'). In e, f-f', Ccn2 is boxed. **g**, **g'**,
826 Representative images (g) and quantification (g') of *Ccn2* expression as determined by HCR. PZ, RZ,
827 GoR: proliferative zone, resting zone, groove of Ranvier (separated from cartilage by dashed line). n= 5
828 Ctl, 5 *Pan-Cart-p21^{MOE}*.

829 **Extended Data Figure 9. a**, **a'**, Mouse model of unilateral, cartilage-targeted, *Ccn2* misexpression (a)
830 and representative H&E images (a') of left and right proximal tibiae at E17.5 (n=3). **b**, **b'**, Representative
831 images (b, boxed regions shown magnified in I-IV) and quantification (b') of Ki67 staining in the RZ of
832 CTL and EXP proximal tibia (n=5 and 3, respectively.)

833 **Extended Data Figure 10.** Comparison of cell proportions between control (CTP) and *Cart-p21* (ETP)
834 samples within the Gli1-lineage (tdTom^{+}). GoR, groove of Ranvier. Note how the RestingChon 2
835 population (arrow) is mainly expanded at the expense of the GoR one.

836 **Conflict of Interest**

837 F.J.R. receives institutional support as a coinvestigator and subcontracted by the Peter MacCallum
838 Cancer Centre for an investigator-initiated trial which receives funding support from Sanofi/Regeneron
839 Pharmaceuticals. The rest of the authors declare that the research was conducted in the absence of any
840 commercial or financial relationships that could be construed as a potential conflict of interest.

841 **Author Contributions**

842 X.Q.: data acquisition and analysis, supervision; E.R.: data acquisition and analysis, figure preparation,
843 manuscript editing; S.L.A.: data analysis, manuscript editing, supervision; K.K.V.: data acquisition and
844 analysis, figure preparation; F.J.R.: data analysis; M.Z.: data analysis; L.G.M.: experimental design, data
845 acquisition; C.H.H.: data analysis, manuscript editing; D.R.P.: tool generation, data analysis,
846 supervision; A.R-D.: conceptualization, experimental design, data analysis, funding acquisition,
847 supervision, figure preparation, manuscript drafting.

848 **Funding**

849 HFSP CDA00021/2019-C (to A.R-D.) and NHMRC Ideas grant 2002084 (to A.R-D. and C.H.H.). The
850 Australian Regenerative Medicine Institute is supported by grants from the State Government of Victoria
851 and the Australian Government. The Novo Nordisk Foundation Center for Stem Cell Medicine, reNEW,
852 is supported by a Novo Nordisk Foundation grant number NNF21CC0073729.

853 **Acknowledgments**

854 We acknowledge the Monash Genomics and Bioinformatics Platform for their excellent technical help,
855 as well as the Monash Genome Modification Platform, for their help with gene targeting and genotyping
856 strategy (design and execution). We thank Timothy Semple for his help with library preparation for the
857 snRNA-seq dataset, and Ricky Johnstone for providing access to bioinformatics expertise.

858 **Data Availability Statement**

859 The single-nuclei and single-cell RNA-seq datasets have been deposited at the NCBI Sequence Read
860 Archive (SRA) with accession numbers PRJNA1136579 and PRJNA1138445, respectively. These can
861 be accessed via the Gene Expression Omnibus (GEO), with accession numbers GSE273540 and
862 GSE273538, respectively.

863 **References**

864 1 Wong, M. & Gilmour, D. Getting back on track: exploiting canalization to uncover the
865 mechanisms of developmental robustness. *Curr Opin Genet Dev* **63**, 53-60 (2020).
866 https://doi.org:10.1016/j.gde.2020.04.001

867 2 Rolian, C. Endochondral ossification and the evolution of limb proportions. *Wiley*
868 *interdisciplinary reviews. Developmental biology*, e373 (2020).
869 https://doi.org:10.1002/wdev.373

870 3 Kronenberg, H. M. Developmental regulation of the growth plate. *Nature* **423**, 332-336 (2003).
871 https://doi.org:10.1038/nature01657

872 4 Zhou, X. *et al.* Chondrocytes transdifferentiate into osteoblasts in endochondral bone during
873 development, postnatal growth and fracture healing in mice. *PLoS Genet* **10**, e1004820 (2014).
874 https://doi.org:10.1371/journal.pgen.1004820

875 5 Maes, C. *et al.* Osteoblast precursors, but not mature osteoblasts, move into developing and
876 fractured bones along with invading blood vessels. *Dev Cell* **19**, 329-344 (2010).
877 https://doi.org:10.1016/j.devcel.2010.07.010

878 6 Karlsson, C., Thornemo, M., Henriksson, H. B. & Lindahl, A. Identification of a stem cell
879 niche in the zone of Ranvier within the knee joint. *J Anat* **215**, 355-363 (2009).
880 https://doi.org:10.1111/j.1469-7580.2009.01115.x

881 7 Newton, P. T. *et al.* A radical switch in clonality reveals a stem cell niche in the epiphyseal
882 growth plate. *Nature* **567**, 234-238 (2019). https://doi.org:10.1038/s41586-019-0989-6

883 8 Harper, J. W., Adami, G. R., Wei, N., Keyomarsi, K. & Elledge, S. J. The p21 Cdk-interacting
884 protein Cip1 is a potent inhibitor of G1 cyclin-dependent kinases. *Cell* **75**, 805-816 (1993).

885 9 Shiratori, H., Yashiro, K., Shen, M. M. & Hamada, H. Conserved regulation and role of Pitx2
886 in situs-specific morphogenesis of visceral organs. *Development* **133**, 3015-3025 (2006).
887 https://doi.org:10.1242/dev.02470

888 10 Posey, K. L. *et al.* An inducible cartilage oligomeric matrix protein mouse model recapitulates
889 human pseudoachondroplasia phenotype. *Am J Pathol* **175**, 1555-1563 (2009).
890 https://doi.org:10.2353/ajpath.2009.090184

891 11 Rosello-Diez, A., Madisen, L., Bastide, S., Zeng, H. & Joyner, A. L. Cell-nonautonomous local
892 and systemic responses to cell arrest enable long-bone catch-up growth in developing mice.
893 *PLoS Biol* **16**, e2005086 (2018). https://doi.org:10.1371/journal.pbio.2005086

894 12 Aibar, S. *et al.* SCENIC: single-cell regulatory network inference and clustering. *Nature*
895 *methods* **14**, 1083-1086 (2017). https://doi.org:10.1038/nmeth.4463

896 13 Shi, Y. *et al.* Gli1 identifies osteogenic progenitors for bone formation and fracture repair.
897 *Nature communications* **8**, 2043 (2017). https://doi.org:10.1038/s41467-017-02171-2

898 14 Phipson, B. *et al.* propeller: testing for differences in cell type proportions in single cell data.
899 *Bioinformatics* **38**, 4720-4726 (2022). https://doi.org:10.1093/bioinformatics/btac582

900 15 Ahmadzadeh, E. *et al.* A collection of genetic mouse lines and related tools for inducible and
901 reversible intersectional misexpression. *Development* **147** (2020).
902 https://doi.org:10.1242/dev.186650

903 16 Ahn, S. & Joyner, A. L. Dynamic changes in the response of cells to positive hedgehog
904 signaling during mouse limb patterning. *Cell* **118**, 505-516 (2004).
905 https://doi.org:10.1016/j.cell.2004.07.023

906 17 Madisen, L. *et al.* A robust and high-throughput Cre reporting and characterization system for
907 the whole mouse brain. *Nat Neurosci* **13**, 133-140 (2010). https://doi.org:10.1038/nn.2467

908 18 Abad, V. *et al.* The role of the resting zone in growth plate chondrogenesis. *Endocrinology*
909 **143**, 1851-1857 (2002). https://doi.org:10.1210/endo.143.5.8776

910 19 H'ng, C. H. *et al.* Compensatory growth and recovery of cartilage cytoarchitecture after
911 transient cell death in fetal mouse limbs. *Nature communications* **15**, 2940 (2024).
912 https://doi.org:10.1038/s41467-024-47311-7

913 20 Li, B. *et al.* Gli1 labels progenitors during chondrogenesis in postnatal mice. *EMBO reports*
914 (2024). https://doi.org:10.1038/s44319-024-00093-x

915 21 He, M. *et al.* Strategies and Tools for Combinatorial Targeting of GABAergic Neurons in
916 Mouse Cerebral Cortex. *Neuron* **92**, 555 (2016). https://doi.org:10.1016/j.neuron.2016.10.009

917 22 Fenichel, I., Evron, Z. & Nevo, Z. The perichondrial ring as a reservoir for precartilaginous
918 cells. In vivo model in young chicks' epiphysis. *Int Orthop* **30**, 353-356 (2006).
919 https://doi.org:10.1007/s00264-006-0082-2

920 23 Chung, M. I., Bujnis, M., Barkauskas, C. E., Kobayashi, Y. & Hogan, B. L. M. Niche-mediated
921 BMP/SMAD signaling regulates lung alveolar stem cell proliferation and differentiation.
922 *Development* **145** (2018). https://doi.org:10.1242/dev.163014

923 24 Squair, J. W. *et al.* Confronting false discoveries in single-cell differential expression. *Nature*
924 *communications* **12**, 5692 (2021). https://doi.org:10.1038/s41467-021-25960-2

925 25 Guo, F., Carter, D. E. & Leask, A. Mechanical tension increases CCN2/CTGF expression and
926 proliferation in gingival fibroblasts via a TGFbeta-dependent mechanism. *PLoS One* **6**, e19756
927 (2011). https://doi.org:10.1371/journal.pone.0019756

928 26 Kubota, S. & Takigawa, M. The role of CCN2 in cartilage and bone development. *J. Cell*
929 *Commun. Signal.* **5**, 209-217 (2011). https://doi.org:10.1007/s12079-011-0123-5

930 27 Nishida, T., Maeda, A., Kubota, S. & Takigawa, M. Role of mechanical-stress inducible
931 protein Hcs24/CTGF/CCN2 in cartilage growth and regeneration: mechanical stress induces
932 expression of Hcs24/CTGF/CCN2 in a human chondrocytic cell line HCS-2/8, rabbit costal
933 chondrocytes and meniscus tissue cells. *Biorheology* **45**, 289-299 (2008).

934 28 Browaeys, R. *et al.* MultiNicheNet: a flexible framework for differential cell-cell
935 communication analysis from multi-sample multi-condition single-cell transcriptomics data.
936 *bioRxiv* (2023).

937 29 Takigawa, M. CCN2: a master regulator of the genesis of bone and cartilage. *Journal of cell*
938 *communication and signaling* **7**, 191-201 (2013). https://doi.org:10.1007/s12079-013-0204-8

939 30 Mizuhashi, K. *et al.* Resting zone of the growth plate houses a unique class of skeletal stem
940 cells. *Nature* **563**, 254-258 (2018). https://doi.org:10.1038/s41586-018-0662-5

941 31 Muruganandan, S. *et al.* A FoxA2+ long-term stem cell population is necessary for growth
942 plate cartilage regeneration after injury. *Nature communications* **13**, 2515 (2022).
943 https://doi.org:10.1038/s41467-022-30247-1

944 32 Chan, L. L., Huang, J., Hagiwara, Y., Aguila, L. & Rowe, D. Discriminating multiplexed GFP
945 reporters in primary articular chondrocyte cultures using image cytometry. *J Fluoresc* **24**,
946 1041-1053 (2014). https://doi.org:10.1007/s10895-014-1383-2

947 33 Ahn, S. & Joyner, A. L. In vivo analysis of quiescent adult neural stem cells responding to
948 Sonic hedgehog. *Nature* **437**, 894-897 (2005). https://doi.org:10.1038/nature03994

34 Hamilton, T. G., Klinghoffer, R. A., Corrin, P. D. & Soriano, P. Evolutionary divergence of platelet-derived growth factor alpha receptor signaling mechanisms. *Mol Cell Biol* **23**, 4013-4025 (2003). https://doi.org:10.1128/MCB.23.11.4013-4025.2003

35 Pei, W. *et al.* Polylox barcoding reveals haematopoietic stem cell fates realized in vivo. *Nature* **548**, 456-460 (2017). https://doi.org:10.1038/nature23653

36 Zhang, B. *et al.* A human embryonic limb cell atlas resolved in space and time. *Nature* (2023). https://doi.org:10.1038/s41586-023-06806-x

37 McGinnis, C. S., Murrow, L. M. & Gartner, Z. J. DoubletFinder: doublet detection in single-cell RNA sequencing data using artificial nearest neighbors. *Cell systems* **8**, 329-337. e324 (2019).

38 Browaeys, R. *et al.* MultiNicheNet: a flexible framework for differential cell-cell communication analysis from multi-sample multi-condition single-cell transcriptomics data. *BioRxiv*, 2023.2006. 2013.544751 (2023).

39 Aibar, S. *et al.* SCENIC: single-cell regulatory network inference and clustering. *Nature methods* **14**, 1083-1086 (2017).

40 Van de Sande, B. *et al.* A scalable SCENIC workflow for single-cell gene regulatory network analysis. *Nature protocols* **15**, 2247-2276 (2020).

41 Beltran Diaz, S. *et al.* A new pipeline to automatically segment and semi-automatically measure bone length on 3D models obtained by Computed Tomography. *Frontiers in Cell and Developmental Biology* (2021). https://doi.org:10.3389/fcell.2021.736574